FORSCHUNGSZENTRUM KARLSRUHE

Technik und Umwelt

Wissenschaftliche Berichte

FZKA 6484

Stress intensity factors and T-stress for cracked circular disks

T. Fett

Institut für Materialforschung

Forschungszentrum Karlsruhe GmbH, Karlsruhe

2000

Stress intensity factors and T-stress for cracked circular disks

Abstract:

The failure of cracked components is governed by the stresses in the vicinity of the crack tip. The singular stress contribution is characterised by the stress intensity factor *K*, the first regular stress term is represented by the so-called *T*-stress.

Stress intensity factors and T-stress solutions for components containing an internal crack were computed predominantly by application of the Boundary Collocation Method (BCM). The results are compiled in the form of tables or approximative relations. In some cases also the fracture mechanics weight function for *K* and a Green's function for *T*-stresses are given, and higher order stress function coefficients are compiled.

Different mechanical boundary conditions are considered: pure traction conditions, mixed boundary conditions and pure displacement conditions.

Spannungsintensitätsfaktoren und T-Spannungsterme für Kreisscheiben mit Rissen

Kurzfassung:

Das Versagen von Bauteilen mit Rissen wird durch die unmittelbar an der Rißspitze auftretenden Spannungen verursacht. Der singuläre Anteil dieser Spannungen wird durch den Spannungsintensitätsfaktor *K* charakterisiert. Der erste reguläre Term wird durch die sogenannte *T*-Spannung beschrieben.

Im vorliegenden Bericht werden Ergebnisse von *K* und *T* für den Fall von Kreisscheiben mit Rissen mitgeteilt, die überwiegend mit der "Boundary Collocation Methode" (BCM) bestimmt wurden. Die Resultate werden in Form von Tabellen und Näherungsformeln wiedergegeben. Zusätzlich wird in einigen Fällen die bruchmechanische Gewichtsfunktion für *K* sowie eine Greensfunktion für *T* angegeben. Auch Koeffizienten für höhere Terme der Spannungsfunktionen werden tabellarisch angegeben.

Als mechanische Randbedingungen werden gewählt: Spannungsrandbedingungen, gemischte Randbedingungen sowie reine Verschiebungsrandbedingungen.

Contents

1 Introduction

While stress intensity factor solutions are reported in handbooks [1-6] for many crack geometries and traction loading cases, weight functions and T-stress solutions are seldom available [5,6]. In most references only solutions for pure traction boundary conditions are reported. In this report also mixed and pure displacement boundary conditions are included. In special cases it may be of advantage to know higher coefficients of the stress series expansion as well. This is desirable e.g. for the computation of stresses over a somewhat wider distance from a crack tip. Therefore, additional coefficients are compiled in some cases.

1.1 Stresses in a cracked body

The complete stress state in a cracked body is known, if a related stress function is known. In most cases, the Airy stress function Φ is an appropriate tool, which results as the solution of

$$\Delta\Delta\Phi = 0 \quad , \quad \Phi = \Phi_s + \Phi_a \tag{1.1}$$

For a cracked body a series representation for Φ was given by Williams [7]. Its symmetric part Φ_s can be written in polar coordinates with the crack tip as the origin

$$\Phi_s = \sigma^* W^2 \sum_{n=0}^{\infty} (r/W)^{n+3/2} A_n \left[\cos(n+\tfrac{3}{2})\varphi - \frac{n+\frac{3}{2}}{n-\frac{1}{2}} \cos(n-\tfrac{1}{2})\varphi \right]$$

$$+\sigma^* W^2 \sum_{n=0}^{\infty} (r/W)^{n+2} A^*_n [\cos(n+2)\varphi - \cos n\varphi] \tag{1.2}$$

and the antisymmetric part Φ_a

$$\Phi_a = \sigma^* W^2 \sum_{n=0}^{\infty} (r/W)^{n+3/2} B_n [\sin(n+\tfrac{3}{2})\varphi - \sin(n-\tfrac{1}{2})\varphi]$$

$$+\sigma^* W^2 \sum_{n=0}^{\infty} (r/W)^{n+2} B^*_n \left[\sin(n+3)\varphi - \frac{n+3}{n+1} \sin(n+1)\varphi \right] \tag{1.2'}$$

where σ^* is a characteristic stress and W is a characteristic dimension. The geometric data are explained by Fig. 1.1. In all mode-I considerations the symmetric part has to be used exclusively. For pure mode-II loadings the antisymmetric part must be applied.
In the symmetric case, the stress components are given by

$$\frac{\sigma_r}{\sigma^*} = \sum_{n=0}^{\infty} A_n (r/W)^{n-1/2} (n+3/2) \left[\frac{n^2 - 2n - 5/4}{n - 1/2} \cos(n-1/2)\varphi - (n+1/2)\cos(n+3/2)\varphi \right]$$

$$+ \sum_{n=0}^{\infty} A^*{}_n (r/W)^n [(n^2 - n - 2)\cos n\varphi - (n+2)(n+1)\cos(n+2)\varphi] \qquad (1.3)$$

$$\frac{\sigma_\varphi}{\sigma^*} = \sum_{n=0}^{\infty} A_n (r/W)^{n-1/2} (n+3/2)(n+1/2) \left[\cos(n+3/2)\varphi - \frac{n+3/2}{n-1/2} \cos(n-1/2)\varphi \right]$$

$$+ \sum_{n=0}^{\infty} A^*{}_n (r/W)^n (n+2)(n+1)[\cos(n+2)\varphi - \cos n\varphi] \qquad (1.4)$$

$$\frac{\tau_{r\varphi}}{\sigma^*} = \sum_{n=0}^{\infty} A_n (r/W)^{n-1/2} (n+3/2)(n+1/2)[\sin(n+3/2)\varphi - \sin(n-1/2)\varphi]$$

$$+ \sum_{n=0}^{\infty} A^*{}_n (r/W)^n (n+1)[(n+2)\sin(n+2)\varphi - n\sin n\varphi] \qquad (1.5)$$

The displacements $u_x = u$ and $u_y = v$ read

$$\frac{u}{\sigma^* W} = \frac{1+\nu}{E} \sum_{n=0}^{\infty} A_n \left(\frac{r}{W} \right)^{n+1/2} \frac{2n+3}{2n-1} [(n + 4\nu - \tfrac{5}{2})\cos(n - \tfrac{1}{2})\varphi - (n - \tfrac{1}{2})\cos(n + \tfrac{3}{2})\varphi] +$$

$$+ \frac{1+\nu}{E} \sum_{n=0}^{\infty} A^*{}_n \left(\frac{r}{W} \right)^{n+1} [(n + 4\nu - 2)\cos n\varphi - (n+2)\cos(n+2)\varphi] \qquad (1.6a)$$

$$\frac{v}{\sigma^* W} = \frac{1+\nu}{E} \sum_{n=0}^{\infty} A_n \left(\frac{r}{W} \right)^{n+1/2} \frac{2n+3}{2n-1} [(n - \tfrac{1}{2})\sin(n + \tfrac{3}{2})\varphi - (n - 4\nu + \tfrac{7}{2})\sin(n - \tfrac{1}{2})\varphi] +$$

$$+ \frac{1+\nu}{E} \sum_{n=0}^{\infty} A^*{}_n \left(\frac{r}{W} \right)^{n+1} [(n+2)\sin(n+2)\varphi - (n - 4\nu + 4)\sin n\varphi] \qquad (1.6b)$$

(ν = Poisson's ratio), from which the Cartesian components result as

$$u_x = u\cos\varphi - v\sin\varphi \qquad (1.7a)$$

$$u_y = u\sin\varphi + v\cos\varphi \qquad (1.7b)$$

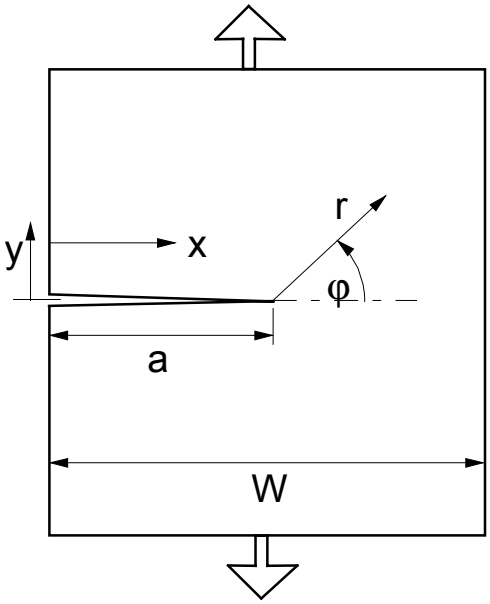

Fig. 1.1 Geometrical data of a crack in a component.

1.2 Stress intensity factor

For the determination of stress intensity factors the Boundary Collocation Method (BCM) and the weight function procedure were applied.
The stress intensity factor K is a measure of the singular stress term occurring near the tip of a crack and defined by

$$\sigma_{ij} = \frac{K}{\sqrt{2\pi a}} f_{ij}(\varphi) \tag{1.8}$$

where r and φ are polar coordinates with the origin at the crack tip.

K is the stress intensity factor. For the loading modes considered in this report the stress intensity factors K_{I} and K_{II} are expressed as

$$K_I = \sigma^* \sqrt{\pi a}\, F_I(a / W) \tag{1.9a}$$

$$K_{II} = \tau^* \sqrt{\pi a}\, F_{II}(a / W) \tag{1.9b}$$

where a is the crack length, W is the width of the component, and σ*, τ* are characteristic stresses in the component, e.g. the outer fibre stress in a bending bar. F_{I} and F_{II} are functions of the ratio of the crack length to the specimen's width as well as of the type of load applied.

The coefficient A_0 in eq.(1.2) is related to the stress intensity factor K_{I} by

$$K_I = \sigma^* 3A_0\sqrt{2\pi W} \tag{1.10}$$

or to the geometric function F_{I} by

$$F_I = A_0\sqrt{18/\alpha} \tag{1.11}$$

with the relative crack depth $\alpha = a/W$.

1.3 T-stress term

Taking into consideration the singular stress term and the first regular term, the near-tip stress field can be described by

$$\sigma_{ij} = \frac{K_I}{\sqrt{2\pi r}} f_{ij}(\varphi) + \sigma_{ij,0} \tag{1.12}$$

$$\sigma_{ij,0} = \begin{pmatrix} \sigma_{xx,0} & \sigma_{xy,0} \\ \sigma_{yx,0} & \sigma_{yy,0} \end{pmatrix} = \begin{pmatrix} T & 0 \\ 0 & 0 \end{pmatrix} \tag{1.13}$$

The term with the coefficient A^*_0 in eq.(1.2) represents the total constant σ_x-stress contribution appearing at the crack tip ($x = a$) of a cracked structure, which is called the T-stress

$$T = \sigma_x\big|_{x=a} = -4\sigma^* A^*_0 \,. \tag{1.14}$$

This total x-stress includes stress contributions which are already present at the location $x = a$ in the uncracked body, $\sigma^{(0)}_{x,a}$, and an additional stress term which is generated by the crack exclusively. This stress separation leads to th definition of two T-stress contributions. The contribution determined by the x-stress in the uncracked structure may be denoted here by $T^{(0)}$

$$T^{(0)} = \sigma^{(0)}_{x,a} \tag{1.15}$$

and the contribution caused by the crack by T_c. Therefore, we can write

$$T = T^{(0)} + T_c \,. \tag{1.16}$$

Leevers and Radon [8] proposed a dimensionless representation of T by the stress biaxiality ratio β, which reads

$$\beta = \frac{T\sqrt{\pi a}}{K_I} = \frac{T}{\sigma^* F} \tag{1.17}$$

or, expressed in terms of stress function coefficients

$$\beta = -\sqrt{\frac{8\alpha}{9}}\,\frac{A^*_0}{A_0} \tag{1.18}$$

Sufficient information about the stress state is available, if the stress intensity factor and the constant stress term, the T-stress, are known. While stress intensity factor solutions are reported in handbooks for many crack geometries and loading cases, T-stress solutions are available only for a small number of test specimens and simple loading cases as for instance pure tension and bending.

Different methods were applied in the past to compute the T-stress term for fracture mechanics standard test specimens. Regarding one-dimensional cracks, Leevers and Radon [8] made a numerical analysis based on a variational method. Kfouri [9] applied the Eshelby technique. Sham [10,11] developed a second-order weight function based on a work-conjugate integral and evaluated it for the SEN specimen using the FE method. In [12,13] a Green's function for T-stresses was determined on the basis of Boundary Collocation results. Wang and Parks [14] extended the T-stress evaluation to two-dimensional surface cracks using the line-spring method. A compilation of results from literature has been given by Sherry et al. [15].

1.4 Weight function

Most of the numerical methods require a separate calculation of the stress intensity factor for each given stress distribution and each crack length. The weight function procedure developed by Bückner [16] simplifies the determination of stress intensity factors. If the weight function is known for a crack in a component, the stress intensity factor can be obtained by multiplying this function by the stress distribution and integrating it along the crack length. The weight function does not depend on the special stress distribution, but only on the geometry of the component.

The method is considered in the following sections for the case of an edge crack. If $\sigma(x)$ is the normal stress distribution and $\tau(x)$ are the shear stresses in the uncracked component along the prospective crack line of an edge crack (Fig. 1.2), the stress intensity factors are given by [16]

$$K_I = \int_0^a h_I(x,a)\,\sigma_n(x)\,dx \tag{1.19a}$$

$$K_{II} = \int_0^a h_{II}(x,a)\,\tau(x)\,dx \tag{1.19b}$$

The general procedures for the determination of weight functions are described below for the weight function component h_I. The relation of Rice [17] allows to determine the weight function from the crack opening displacement $v_r(x,a)$ of any arbitrarily chosen loading and the corresponding stress intensity factor $K_{Ir}(a)$ according to

$$h_I(x,a) = \frac{E'}{K_{Ir}(a)} \frac{\partial v_r(x,a)}{\partial a} \tag{1.20}$$

($E' = E$ for plane stress and $E' = E/(1-\nu^2)$ for plane strain conditions) where the subscript r stands for the reference loading case. It is convenient to use $\sigma_r(x) = \sigma_0 =$ constant for the reference stress distribution.

One possibility to derive the weight function with eq.(1.20) is the evaluation of numerically determined crack opening profiles, which may be obtained by BCM computations. By application of the BCM procedure to a couple of cracks with slightly different lengths a and a+da, a large number of coefficients A_n and A_n* is obtained. Then eq.(1.6a) provides the related

couple of crack opening displacements $v(a)$ and $v(a+da)$. Use of eq.(1.20) yields the weight function. In order to minimise the numerical effort, approximate methods are often used in literature.

1.5 Representation of T-stresses by a Green's function

As a consequence of the principle of superposition, stress fields for different loadings can be added in the case of single loadings acting simultaneously. This leads to an integration representation of the loading parameters and was applied very early to the singular stress field and the computation of the related stress intensity factor by Bückner [16]. Similarly, the T-stress contribution T_c caused by the crack exclusively can be expressed by an integral [10-13]. The integral representation reads

$$T_c = \int_0^a t(x,a)\, \sigma_y(x)\, dx \tag{1.21}$$

where the integration has to be performed with the stress field σ_y in the uncracked body (Fig. 1.2). The stress contributions are weighted by a weight function (h, t) which depends on the location x where the stress σ_y acts.

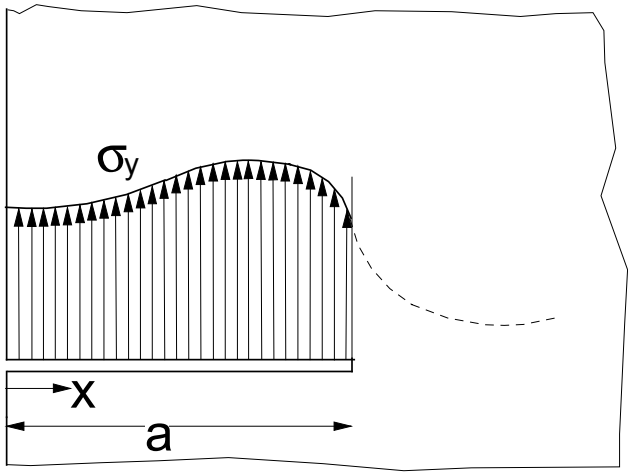

Fig. 1.2 Crack loaded by continuously distributed normal tractions σ_y (present in the uncracked body).

The weight functions h and t can be interpreted as the stress intensity factor and as the T-term for a pair of single forces P acting on the crack face at the location x_0 (Fig. 1.2), i.e. the weight functions (h, t) are Green's functions for K_I and T_c. This can be shown easily. The single forces are represented by a stress distribution

$$\sigma(x) = \frac{P}{B}\delta(x - x_0) \tag{1.22}$$

where δ is the Dirac Delta-function and B is the thickness of the plate (often chosen to be $B = 1$). By introducing this stress distribution into (1.21), we obtain

$$T_P = \frac{P}{B}\int_0^a \delta(x - x_0)\, t(x,a)\, dx = \frac{P}{B} t(x_0, a) \tag{1.23}$$

i.e. the weight function term $t(x_0,a)$ is the Green's function for the T-stress term.

In order to describe the Green's function, it is distinguished between a term t_0 representing the asymptotic limit case of near-tip behaviour and a correction term t_{corr} which includes information about the special shape of the component and the finite dimensions,

$$t = t_0 + t_{corr} \tag{1.24}$$

with [13,18]

$$t_0 = -\frac{1}{\pi}\lim_{x'\to a}\frac{\sqrt{x'-a}}{(x'-x)\sqrt{a-x}}\ . \tag{1.25}$$

$$\Rightarrow \quad T_{c,0} = \int t_0(x', a, x)\,\sigma(x)\, dx = -p\big|_{x=a} = -\sigma_y\big|_{x=a} \tag{1.26}$$

Then the complete Green's function can be written as [13,18]

$$t = t_0 + \sum_{\nu=1}^{\infty} C_\nu (1 - x/a)^\nu \tag{1.27}$$

If we restrict the expansion to the leading term, we obtain as an approximation

$$t \cong t_0 + C\left(1 - \frac{x}{a}\right) \tag{1.28}$$

A simple procedure to determine approximative Green's functions is to determine the unknown coefficients in the series representation (1.27) of known T-solutions for reference loading cases [6].

For internal cracks it holds

$$t = t_0 + \sum_{\nu=1}^{\infty} C_\nu (1 - x^2/a^2)^\nu \tag{1.29}$$

with the first approximation

$$t \cong t_0 + C(1 - x^2 / a^2) \tag{1.30}$$

In this case, the coefficient C results from the pure tension case as

$$C = \frac{3}{2a}\left(1 + \frac{T_t}{\sigma_0}\right) \tag{1.31}$$

In order to improve the Green's function, the next regular term is added. Consequently, the Green's function expansion reads for edge cracks

$$t(x) = t_0 + C_1(1 - x / a) + C_2(1 - x / a)^2 \tag{1.32}$$

or

$$T_c = -\sigma_y\big|_{x=a} + C_1 \int_0^a \sigma_y(x)(1 - x / a)\, dx + C_2 \int_0^a \sigma_y(x)(1 - x / a)^2\, dx \tag{1.33}$$

For internal cracks it holds

$$t = t_0 + C_1(1 - x^2 / a^2) + C_2(1 - x^2 / a^2)^2 \tag{1.34}$$

The determination of the two coefficients C_1 and C_2 is possible, if T-stress solutions for two different reference loading cases are available.

2 Circular disk with internal crack

2.1 Constant load

The circular disk with a symmetrical internal crack is shown in Fig 2.1.1.

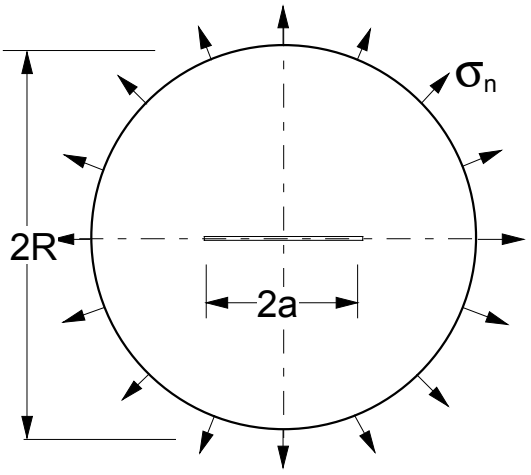

Fig. 2.1.1 Circular disk with internal crack under constant normal tractions at the circumference.

The crack under constant circumferential tractions (Fig. 2.1.1) has been analysed with the Boundary Collocation method.

The stress intensity factor solution is [6]

$$F = \frac{K}{\sigma_n \sqrt{\pi a}} = \frac{1 - 0.5\alpha + 1.6873\alpha^2 - 2.671\alpha^3 + 3.2027\alpha^4 - 1.8935\alpha^5}{\sqrt{1-\alpha}}. \qquad (2.1.1)$$

The T-stress terms can be approximated by

$$T_c / \sigma = \frac{-1 + \alpha - 2.34\alpha^2 + 4.27\alpha^3 - 3.326\alpha^4 + 0.9824\alpha^5}{1-\alpha} \qquad (2.1.2)$$

$$T / \sigma = \frac{-2.34\alpha^2 + 4.27\alpha^3 - 3.326\alpha^4 + 0.9824\alpha^5}{1-\alpha} \qquad (2.1.3)$$

The T-values in Table 2.1.1 were extrapolated to $\alpha = 1$. Within the numerical accuracy of the extrapolation, the limit values are

$$\lim_{\alpha\to 1} T / \sigma^*(1-\alpha) = \lim_{\alpha\to 1} T_c / \sigma^*(1-\alpha) \cong -0.413 = -\frac{1}{\sqrt{\pi^2 - 4}} \tag{2.1.4}$$

and for the biaxiality ratio

$$\lim_{\alpha\to 1} \beta\sqrt{1-\alpha} \cong \frac{1}{2} \tag{2.1.5}$$

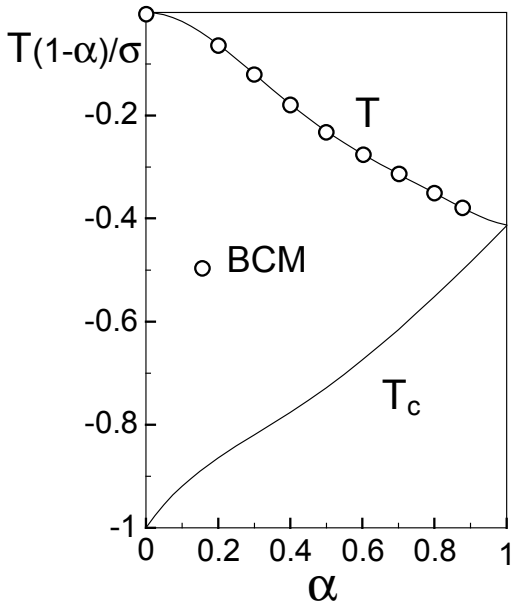

Fig. 2.1.2 T-stress for an internal crack in a circular disk.

$\alpha = a/R$	$T_c/\sigma\cdot(1-\alpha)$	$T/\sigma\cdot(1-\alpha)$	$F\cdot(1-\alpha)^{1/2}$	$\beta\cdot(1-\alpha)^{1/2}$
0	-1.00	0.000	1.000	0.00
0.1	-0.919	-0.019	0.965	-0.020
0.2	-0.864	-0.064	0.951	-0.067
0.3	-0.820	-0.120	0.951	-0.126
0.4	-0.776	-0.176	0.962	-0.183
0.5	-0.728	-0.228	0.979	-0.233
0.6	-0.675	-0.275	0.998	-0.275
0.7	-0.615	-0.315	1.011	-0.311
0.8	-0.552	-0.352	1.004	-0.351
0.9	-0.485	-0.385	0.953	-0.404
1.0	-0.413	-0.413	0.8255	-0.50

Table 2.1.1 T-stress, stress intensity factor, and biaxiality ratio for an internally cracked circular disk with constant tensile tractions at the circumference (value T for $\alpha = 1$ extrapolated); for T and T_c see eqs.(1.15) and (1.16).

Figure 2.1.3 represents the displacement at $x = 0$ under constant normal tractions σ_n in the form

$$\delta = \frac{2a\sigma_n}{E'} \frac{1}{\alpha} \ln \frac{1}{1-\alpha} \lambda(\alpha) \quad , \quad \alpha = a / R \tag{2.1.6}$$

The open circles result from Boundary Collocation computations and the solid curve is the result obtained by application of the procedure proposed by Paris (see e.g. Appendix B in Tadas handbook [1]). The solid circles are analytical values resulting from limit case considerations [1]. The dashed curve in Fig. 2.1.3 is the solution for the endless parallel strip with an internal crack as reported by Tada [1].

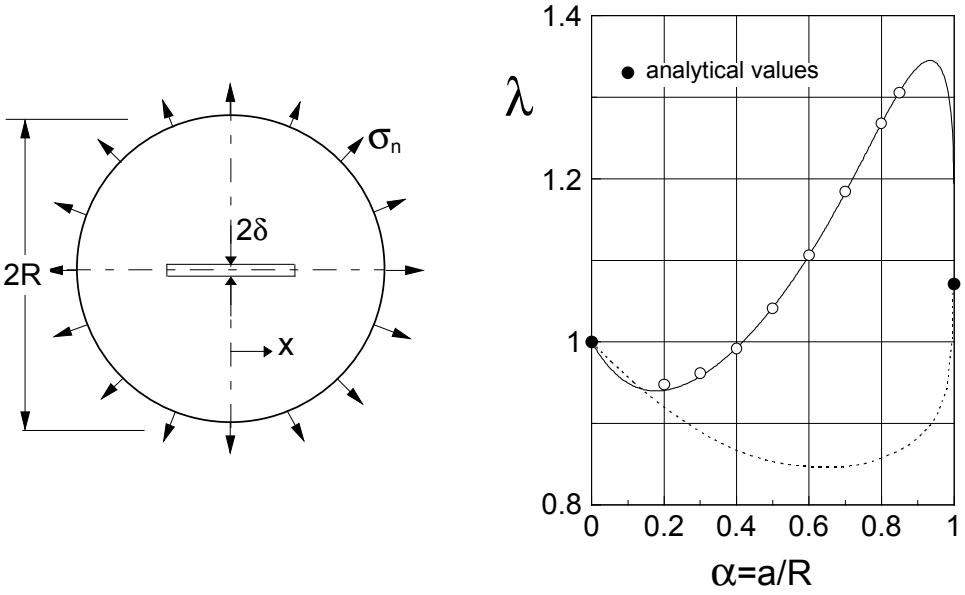

Fig. 2.1.3 Crack opening displacements for the internally cracked disk according to eq.(2.1.6) (circles: BCM-results, solid curve: procedure of Paris). Dashed line: data for an internally cracked endless strip [1].

2.2 Disk partially loaded by normal tractions at the circumference

A partially loaded disk is shown in Fig. 2.2.1a. Constant normal tractions σ_n are applied at the circumference within an angle of 2γ.

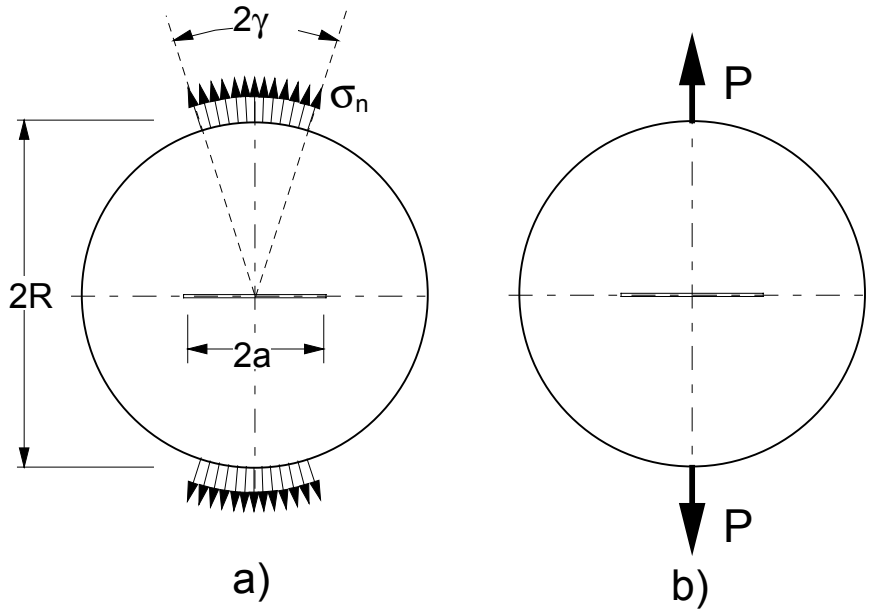

Fig. 2.2.1 a) partially loaded disk, b) diametral loading by a couple of forces (disk thickness: *t*).

The total force in *y*-direction results from

$$P_y = 2t\sigma_n \int_0^{\gamma} R\cos\gamma' \, d\gamma' = 2t\sigma_n R\sin\gamma \tag{2.2.1}$$

The geometric function *F* defined by

$$K_I = \sigma^* \sqrt{\pi a}\, F(a/R) \tag{2.2.2}$$

is plotted in Fig. 2.2.2, with σ^* defined as

$$\sigma^* = \frac{P_y}{\pi R t}\ , \tag{2.2.3}$$

From the limit case $\gamma \to 0$, the solutions for concentrated forces (see Fig. 2.2.1b) are obtained as represented in Fig. 2.2.3. A comparison with the results from literature [19-21] yields a good agreement of the stress intensity factors. The solution given by Tada et al. [1] (dashed curve in Fig. 2.2.3) deviates by about 20% near a/R=0.8. The results obtained here can be expressed by

$$K_I = \sigma^* \sqrt{\pi a} F_P \quad , \quad F_P = \frac{3 - 1.254\,\alpha - 1.7013\,\alpha^2 + 4.0597\,\alpha^3 - 2.8059\,\alpha^4}{\sqrt{1-\alpha}} \tag{2.2.4}$$

with σ^* given in (2.2.3).

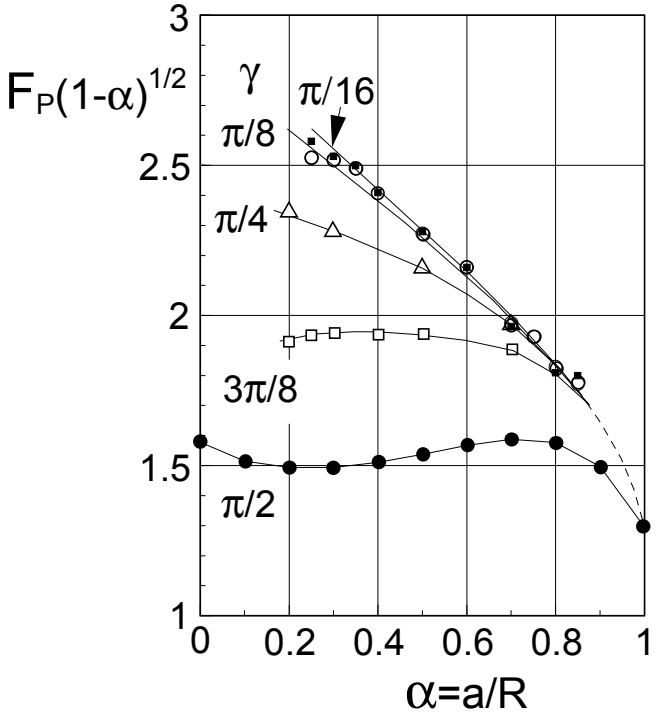

Fig. 2.2.2 Stress intensity factors for a circular disk, partially loaded over an angle of 2γ (see Fig.2.2.1a).

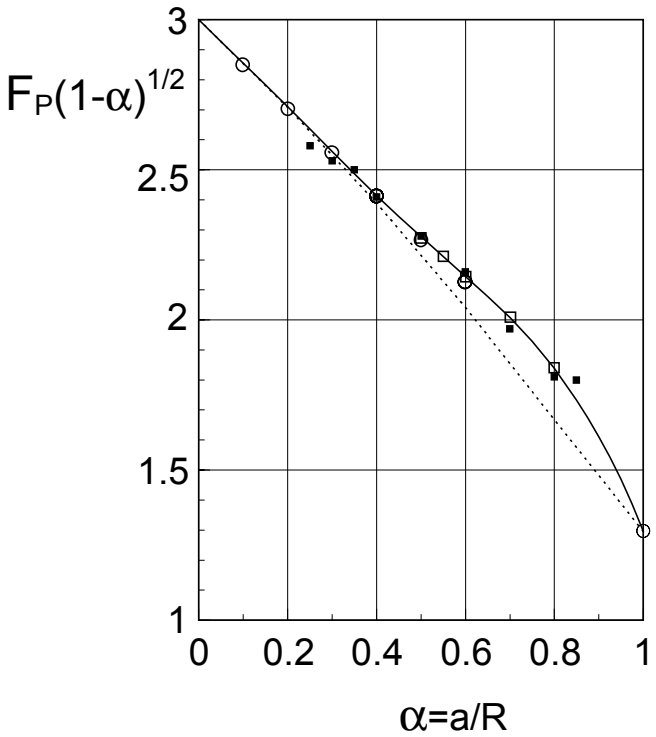

Fig. 2.2.3 Stress intensity factor and T-stress for a circular disk loaded diametrically by concentrated forces (Fig. 2.2.1b). Comparison of stress intensity factors; solid squares: partially distributed stresses with an angle of γ=π/16, circles: results by Atkinson et al. [19] and Awaji and Sato [20], open squares: results obtained with the weight function technique [21], dashed line: solution proposed by Tada et al.[1].

The x-stress term T, normalised to σ*, is shown in Fig. 2.2.4. From the limit case γ→0, the solutions for concentrated forces (see Fig. 2.2.1b) are obtained as represented in Fig. 2.2.5.

The T-stress can be fitted by

$$\frac{T}{\sigma^*} = \frac{-4(1-\alpha) + 7.6777\,\alpha^2 - 16.0169\,\alpha^3 + 8.7994\,\alpha^4 - 1.10849\,\alpha^5}{1-\alpha} \tag{2.2.5}$$

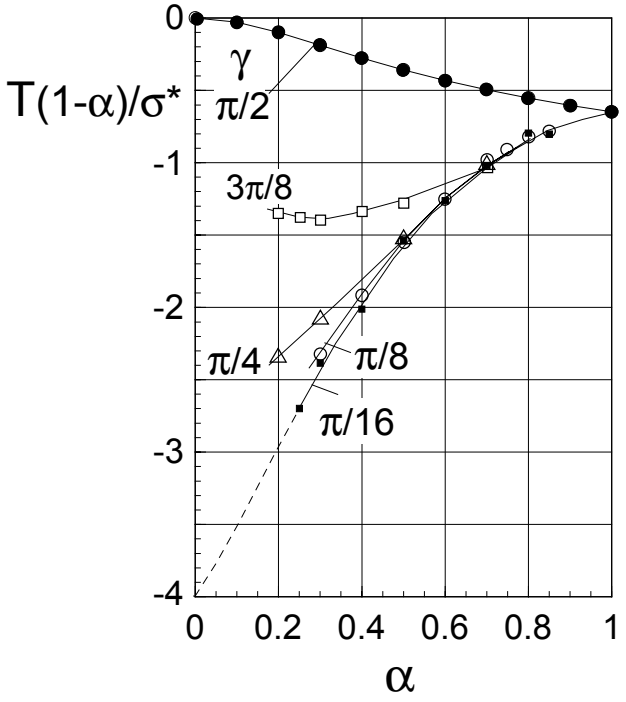

Fig. 2.2.4 T-stress for a circular disk, partially loaded over an angle of 2γ (see Fig. 2.2.1a).

T_c can be computed from T

$$\frac{T_c}{\sigma^*} = \frac{-3(1-\alpha) + 7.6777\,\alpha^2 - 16.0169\,\alpha^3 + 8.7994\,\alpha^4 - 1.10849\,\alpha^5}{1-\alpha} - \frac{4\alpha^2}{(1+\alpha^2)^2} \tag{2.2.6}$$

or expressed by a fit relation

$$\frac{T_c}{\sigma^*} \cong \frac{-3(1-\alpha) + 2.8996\,\alpha^2 - 6.1759\,\alpha^3 + 2.5438\,\alpha^4 + 0.0841\,\alpha^5}{1-\alpha} \tag{2.2.7}$$

In this case, the limit values are (at least in very good approximation)

$$\lim_{\alpha\to 1} T / \sigma^*(1-\alpha) = \lim_{\alpha\to 1} T_c / \sigma^*(1-\alpha) \cong -0.648 \cong -\frac{\pi}{2\sqrt{\pi^2-4}} \tag{2.2.8}$$

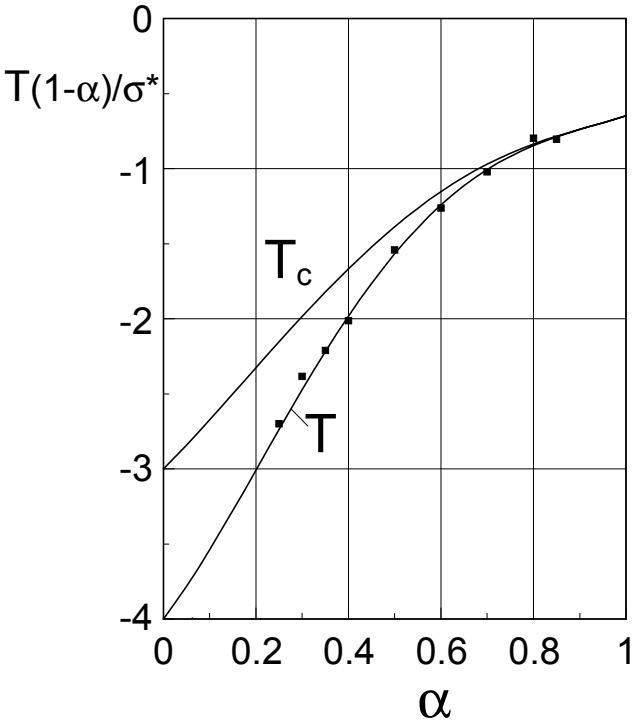

Fig. 2.2.5 T-stress for a circular disk loaded diametrically by concentrated forces (Fig. 2.2.1b). T-stress results including partially distributed stresses with an angle of $\gamma = \pi/16$ (squares) and exact limit cases for $\alpha = 0$.

2.3 Central point force on the crack face

A centrally cracked circular disk, loaded by a couple of forces at the crack centre, is shown in Fig. 2.3.1. For this, the stress intensity factor and the T-stress were calculated by Boundary Collocation computations.

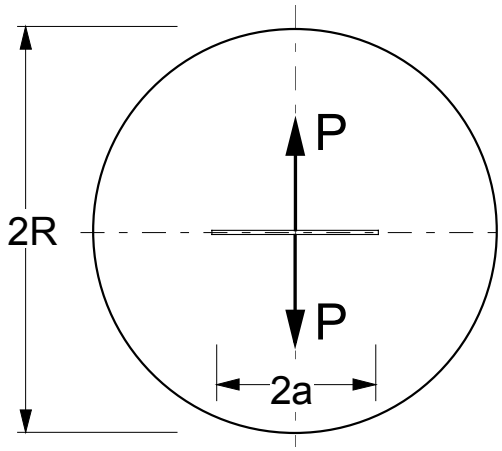

Fig. 2.3.1 Circular disk with a couple of forces acting on the crack faces.

The stress intensity factor for central point forces is

$$K_I = \frac{P}{\sqrt{\pi a}} F_P \tag{2.3.1}$$

$$F_P = \frac{1 - 1.07884\alpha + 8.24956\alpha^2 - 17.9026\alpha^3 + 20.3339\alpha^4 - 9.305\alpha^5}{\sqrt{1-\alpha}}$$

Figure 2.3.2 shows a comparison of the BCM results with results obtained by Tada et al. [1] using an asymptotic extrapolation technique. Maximum differences are in the order of about 10%.

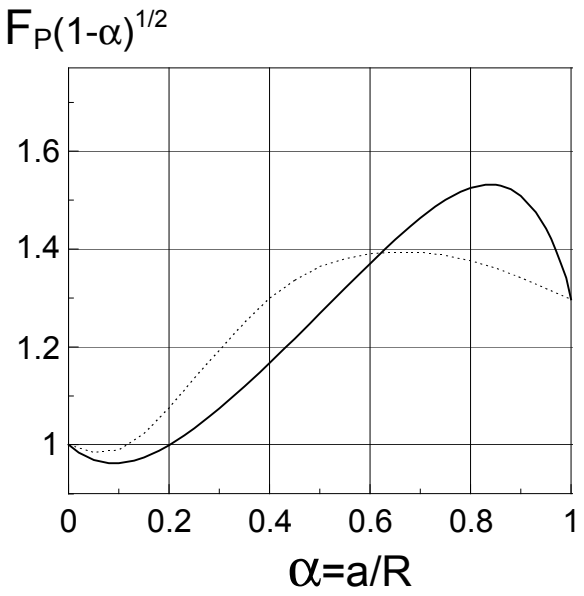

Fig. 2.3.2 Stress intensity factor for a couple of forces P at the crack centre, represented by the geometric function F_P. Solid curve: derived in [22], dashed curve: Tada et al. [1].

The T-stress data obtained with the BCM method are plotted by the squares in Fig. 2.3.3. Together with the limit value, eq.(2.2.8), the numerically found T-values were fitted by the polynomial

$$\frac{T}{\sigma^*} = \frac{-4.1971\alpha + 5.4661\alpha^2 - 1.1497\alpha^3 - 0.7677\alpha^4}{1-\alpha} \tag{2.3.2}$$

This relation is introduced into Fig. 2.3.3 as the solid line.

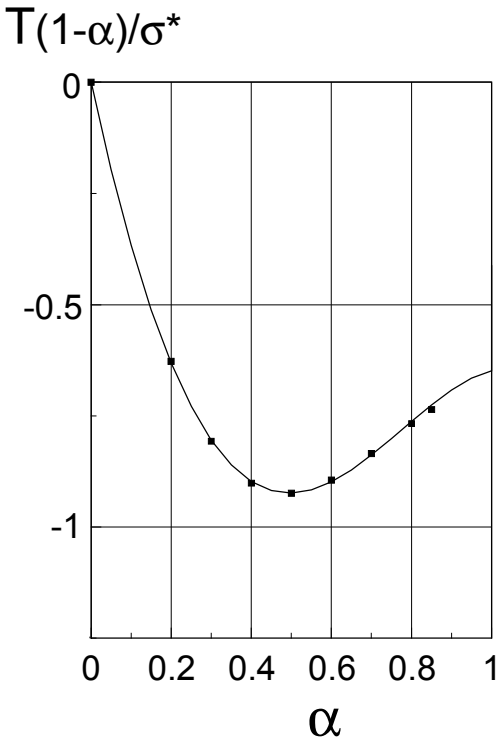

Fig. 2.3.3 T-stress for an internally cracked circular disk with a couple of forces acting in the crack centre on the crack faces [23]. Symbols: numerical results, solid line: fitting curve.

Mode-I weight function [6]

$$h_I = \frac{2}{\sqrt{\pi a}}\left[\frac{1}{\sqrt{1-\rho^2}} + C_0\sqrt{1-\rho^2} + C_1(1-\rho^2)^{3/2}\right] \quad , \rho = x/a \tag{2.3.3}$$

$$C_0 = \frac{8 - 4\alpha + 3.8612\alpha^2 - 15.9344\alpha^3 + 24.6076\alpha^4 - 13.234\alpha^5}{\sqrt{1-\alpha}} - 8 \tag{2.3.4}$$

$$C_1 = -\frac{8 - 4\alpha + 0.6488\alpha^2 - 14.1232\alpha^3 + 24.2696\alpha^4 - 12.596\alpha^5}{\sqrt{1-\alpha}} + 8 \tag{2.3.5}$$

A two-terms Green's function for the T-stress term reads [23]

$$t = t_0 + C_1(1 - x^2/a^2) + C_2(1 - x^2/a^2)^2 \tag{2.3.6}$$

$$C_1 = \frac{1}{R}\,\frac{-6.8622\,\alpha + 18.1057\,\alpha^2 - 22.0173\,\alpha^3 + 9.3229\,\alpha^4}{1-\alpha} \tag{2.3.7}$$

$$C_2 = \frac{1}{R}\,\frac{4.1902\,\alpha - 14.626\,\alpha^2 + 21.2854\,\alpha^3 - 9.8117\,\alpha^4}{1-\alpha} \tag{2.3.8}$$

With the Green's function the diametral tension specimen was computed using the stress distribution (Fig. 2.2.1b)

$$\frac{\sigma_y}{\sigma^*} = \frac{4}{(1+\xi^2)^2} - 1 \quad , \quad \xi = x\,/\,R \tag{2.3.9}$$

$$\frac{\sigma_x}{\sigma^*} = -1 + \frac{4\xi^2}{(1+\xi^2)^2} \tag{2.3.10}$$

The result is plotted in Fig. 2.3.4. It becomes obvious that in this approximation small deviations are only visible for large α.

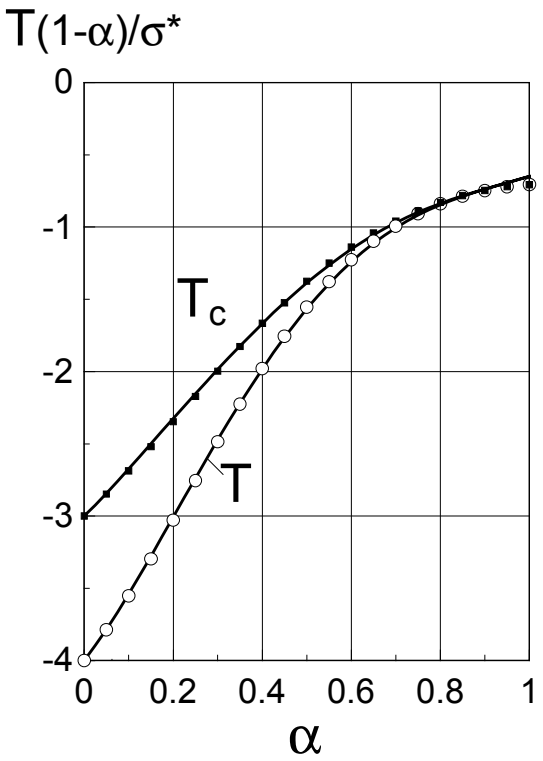

Fig. 2.3.4 T-stresses for an internally cracked circular disk, loaded by a couple of diametral forces at the free boundary (see Fig. 2.2.1b) estimated with the 2-terms Green's function (symbols) compared with results of BCM computations (curves).

2.4 Mode-II loading

Figure 2.4.1 shows the crack-face loading by a constant shear stress τ and a pair of concentrated tangential forces *Q*.

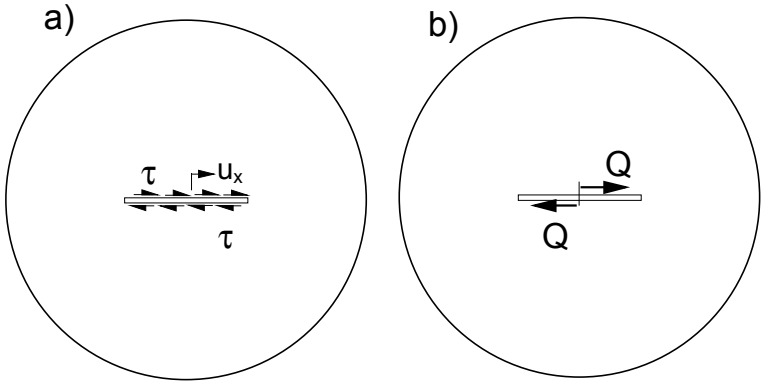

Fig. 2.4.1 Internal radial crack loaded by shear tractions, a) constant shear stress τ, b) pair of concentrated shear forces *Q*.

Stress intensity factor under constant shear tractions τ [21]

$$K_{II} = \tau F_{II}\sqrt{\pi a}\ , \quad F_{II} = \frac{1-0.5\alpha+0.9274\alpha^2-0.88414\alpha^3+0.28226\alpha^4}{\sqrt{1-\alpha}} \tag{2.4.1}$$

with $\alpha = a/R$.

Stress intensity factor for a point load *Q* (line load over plate thickness *t*) in the crack centre [21]

$$K_{II,Q} = \frac{2Q}{t\sqrt{\pi a}} F_{II,Q}\ , \quad F_{II} = \frac{1-0.5\alpha+1.977\alpha^2-1.5655\alpha^3+0.3851\alpha^4}{\sqrt{1-\alpha}}. \tag{2.4.2}$$

A mode-II weight function is [21]

$$h_{II} = \frac{2}{\sqrt{\pi a}}\left[\frac{1}{\sqrt{1-\rho^2}} + D_0\sqrt{1-\rho^2} + D_1(1-\rho^2)^{3/2}\right] \tag{2.4.3}$$

$$D_0 = \frac{5-2.5\alpha+1.4882\alpha^2-2.3766\alpha^3+1.1028\alpha^4}{\sqrt{1-\alpha}} - 5 \tag{2.4.4}$$

$$D_1 = \frac{-4+2\alpha+0.4888\alpha^2+0.81112\alpha^3-0.7177\alpha^4}{\sqrt{1-\alpha}} + 4 \tag{2.4.5}$$

2.5 Brazilian Disk

The mixed-mode loading under diametrically applied concentrated forces is shown in Fig. 2.5.1.

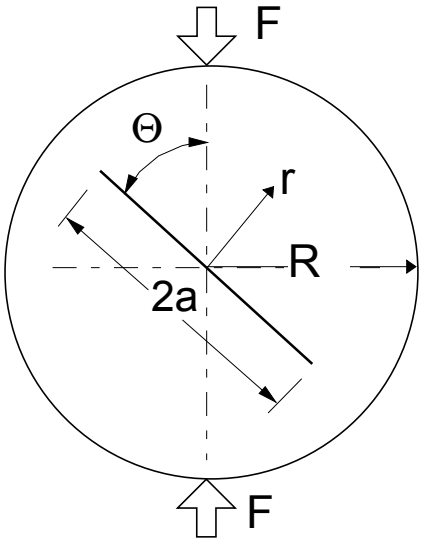

Fig. 2.5.1 Diametral compression test with internal crack (disk thickness: *t*).

The stress intensity factors K_{I}, K_{II} and related geometric functions F_{I}, F_{II} are

$$K_I = \sigma_0 F_I \sqrt{\pi a} = \int_0^a \sigma(x) h_I(x,a)\, dx \tag{2.5.1}$$

$$K_{II} = \sigma_0 F_{II} \sqrt{\pi a} = \int_0^a \tau(x) h_{II}(x,a)\, dx \tag{2.5.2}$$

The characteristic stress is chosen as

$$\sigma_0 = \frac{F}{\pi a t} \quad , \tag{2.5.3}$$

(identical with the maximum tensile stress in the centre of the disk).

The circumferential stress component in an uncracked Brazilian disk has been given by Erdlac (quoted in [19]) as

$$\sigma_\varphi = \sigma_n = \frac{2P}{\pi t R}\left[\frac{1}{2} - \frac{(1-\rho\cos\Theta)\sin^2\Theta}{(1+\rho^2-2\rho\cos\Theta)^2} - \frac{(1+\rho\cos\Theta)\sin^2\Theta}{(1+\rho^2+2\rho\cos\Theta)^2}\right] \tag{2.5.4}$$

$$\sigma_r = \frac{2P}{\pi t R}\left[\frac{1}{2} - \frac{(1-\rho\cos\Theta)(\cos\Theta-\rho)^2}{(1+\rho^2-2\rho\cos\Theta)^2} - \frac{(1+\rho\cos\Theta)(\cos\Theta+\rho)^2}{(1+\rho^2+2\rho\cos\Theta)^2}\right] \tag{2.5.5}$$

with $\rho = r / R$.

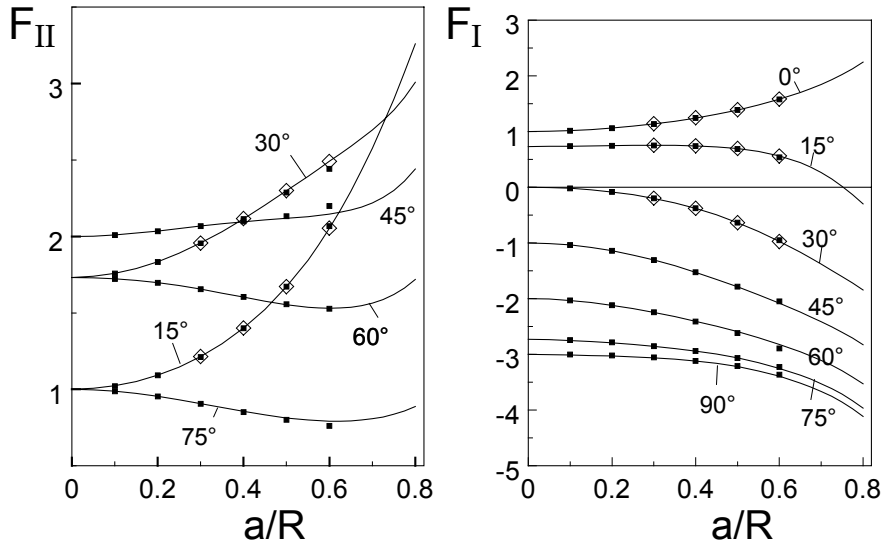

Fig. 2.5.2 Geometric functions for mode-II and mode-I stress intensity factors. Curves: obtained with weight functions [21]; solid squares: Atkinson et al. [19]; open squares: Sato and Kawamata [24].

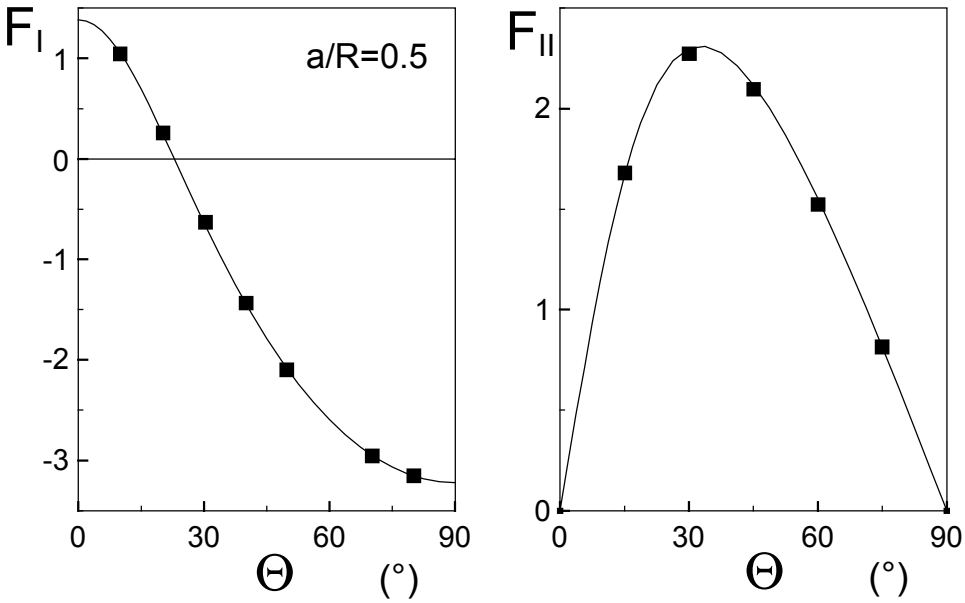

Fig. 2.5.3 Geometric functions for a/R=0.5 as a function of the angle Θ. Curves: obtained with the weight function procedure; squares: results from Atkinson et al. [19] and Awaji and Sato [20].

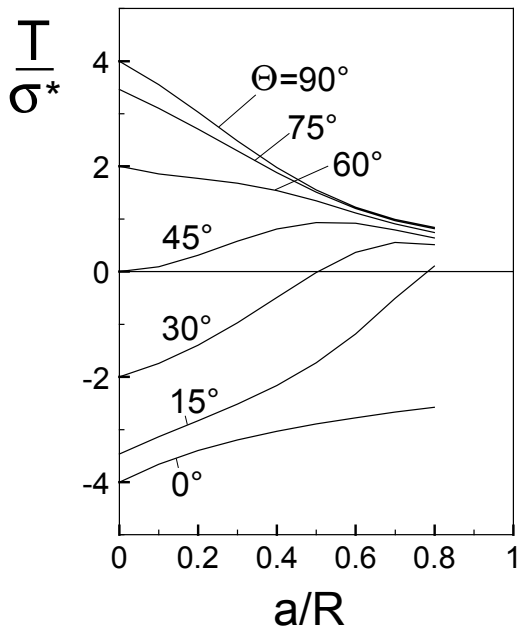

Fig. 2.5.4 T-stress for the Brazilian disk as a function of the angle Θ.

a/*R*	Θ=0°	15°	30°	45°	60°	75°	90°
0	-4.000	-3.464	-2.000	0.000	2.000	3.464	4.000
0.1	-3.656	-3.136	-1.745	0.091	1.855	3.104	3.552
0.2	-3.398	-2.829	-1.396	0.312	1.773	2.711	3.029
0.3	-3.197	-2.515	-0.969	0.581	1.684	2.294	2.485
0.4	-3.033	-2.163	-0.492	0.812	1.543	1.883	1.980
0.5	-2.895	-1.733	-0.015	0.935	1.344	1.509	1.555
0.6	-2.775	-1.183	0.369	0.919	1.116	1.201	1.227
0.7	-2.668	-0.510	0.553	0.795	0.906	0.971	0.993
0.8	-2.574	0.106	0.513	0.643	0.746	0.815	0.839

Table 2.5.1 T-stress $T(1\text{-}a/R)$ for the Brazilian disk test.

a/*R*	Θ=0°	15°	30°	45°	60°	75°	90°
0	0.	1.000	1.732	2.000	1.732	1.000	0.
0.1	0.	1.023	1.758	2.010	1.724	0.988	0.
0.2	0.	1.092	1.835	2.036	1.698	0.955	0.
0.3	0.	1.214	1.957	2.069	1.656	0.907	0.
0.4	0.	1.400	2.116	2.097	1.603	0.856	0.
0.5	0.	1.670	2.299	2.119	1.554	0.813	0.
0.6	0.	2.053	2.491	2.146	1.530	0.792	0.
0.7	0.	2.578	2.697	2.220	1.564	0.808	0.
0.8	0.	3.260	3.009	2.441	1.720	0.889	0.

Table 2.5.2 Geometric function F_{II} for the Brazilian disk tests.

a/R	Θ=0°	15°	30°	45°	60°	75°	90°
0	1.000	0.732	0	-1.000	-2.000	-2.732	-3.000
0.1	1.017	0.737	-0.020	-1.037	-2.033	-2.750	-3.016
0.2	1.063	0.746	-0.084	-1.141	-2.120	-2.793	-3.031
0.3	1.137	0.752	-0.200	-1.308	-2.248	-2.854	-3.062
0.4	1.241	0.742	-0.379	-1.527	-2.406	-2.940	-3.118
0.5	1.384	0.693	-0.635	-1.789	-2.594	-3.065	-3.220
0.6	1.578	0.562	-0.973	-2.083	-2.819	-3.250	-3.393
0.7	1.846	0.263	-1.381	-2.413	-3.108	-3.525	-3.665
0.8	2.244	-0.302	-1.843	-2.824	-3.530	-3.965	-4.112

Table 2.5.3 Geometric function F_1 for the Brazilian disk tests.

2.6 Mixed boundary conditions

Constant radial displacement and disappearing shear tractions

The internally cracked circular disk under constant radial displacement and disappearing shear tractions along the circumference is illustrated in Fig. 2.6.1.

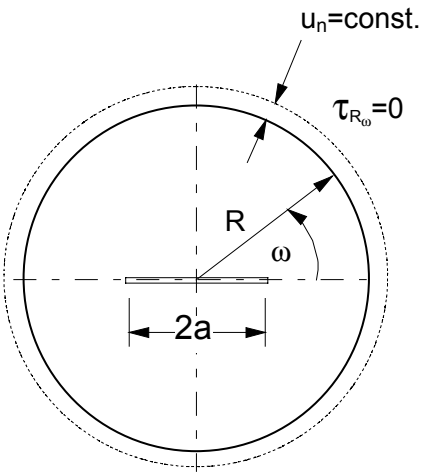

Fig. 2.6.1 Boundary conditions $u_n = u_R$ = constant, $\tau_{R\omega} = 0$.

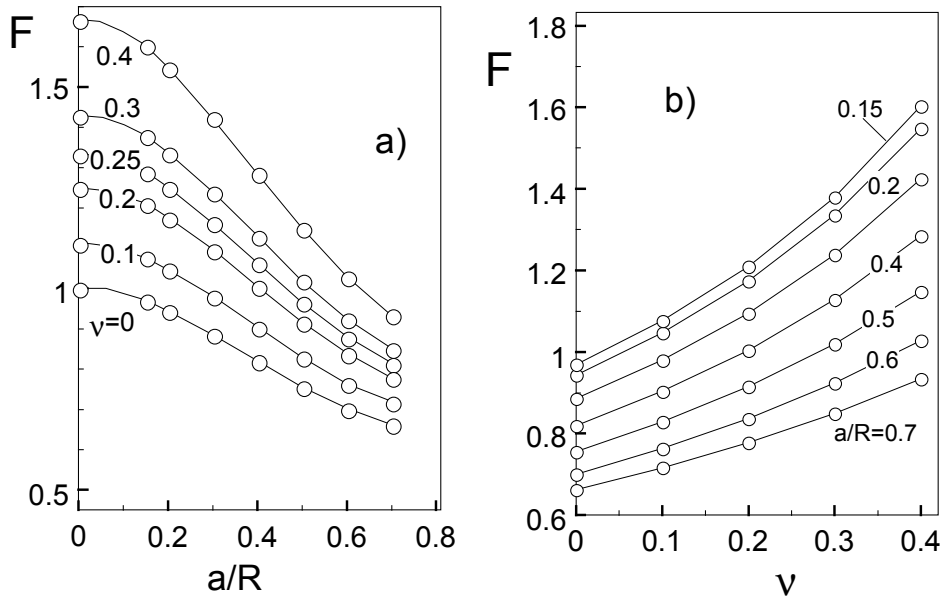

Fig. 2.6.2 Geometric function *F* according to eq.(6.6.1)

The stress intensity factor for the loading case of u_R = constant, $\tau_{R\omega}$=0 is defined by

$$K = \sigma^* \sqrt{\pi a}\, F(a / R, \nu, \gamma) \ , \quad \sigma^* = \frac{u_R E}{R} \tag{2.6.1}$$

The geometric function F is plotted in Fig. 2.6.2 as a function of a/R and ν.
For the special case of $\nu = 0.25$ and $\alpha = a/R \le 0.7$ a fit relation reads

$$F = \tfrac{4}{3} - 2.154\,\alpha^2 + 3.200\alpha^4 - 1.987\alpha^6 \qquad (2.6.2)$$

The T-stress, nomalised to the stress σ*, is represented in Fig. 2.6.3. The higher order coefficients A_1 and A^*_1, see eq.(1.2), are compiled in Tables 2.6.1 and 2.6.2

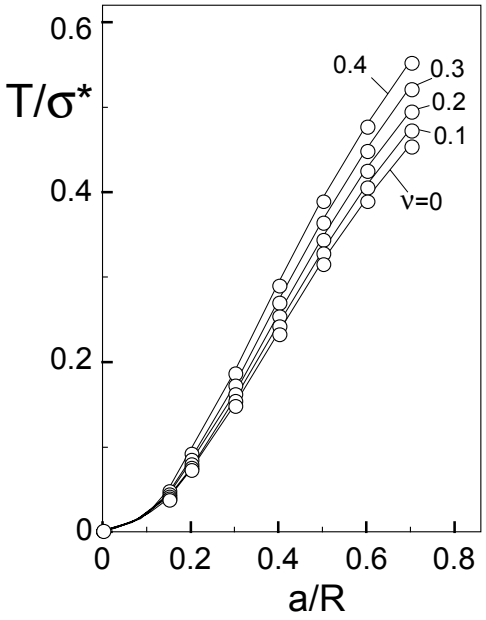

Fig. 2.6.3 T-stress as a function of crack size and Poisson's ratio.

For $\nu = 0.25$ and $\alpha = a/R \le 0.7$ we find

$$T / \sigma^* = 2.597\alpha^2 - 2.685\alpha^3 + 0.6495\alpha^5 \qquad (2.6.3)$$

	ν=0	0.1	0.2	0.3	0.4
a/R=0.15	-0.1255	-0.1393	-0.1565	-0.1784	-0.2073
0.2	-0.1060	-0.1175	-0.1317	-0.1497	-0.1734
0.3	-0.0826	-0.0911	-0.1016	-0.1147	-0.1316
0.4	-0.0692	-0.0757	-0.0836	-0.0933	-0.1056
0.5	-0.0624	-0.0674	-0.0734	-0.0807	-0.0897
0.6	-0.0617	-0.0656	-0.0702	-0.0758	-0.0825
0.7	-0.0689	-0.0722	-0.0760	-0.0805	-0.0858

Table 2.6.1 Coefficient A_1 according to eq.(1.2).

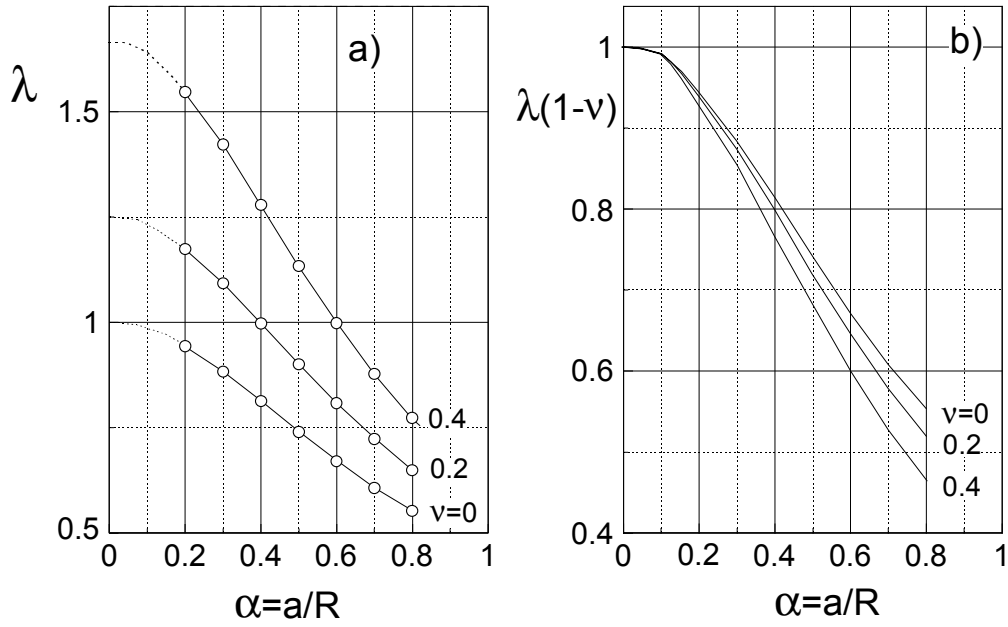

Fig. 2.6.4 Crack opening displacement δ at $x = 0$ (for δ and x see Fig. 2.1.3) as a function of Poisson's ratio.

The crack opening displacements at $x = 0$, represented as

$$\delta = \frac{2a\sigma^*}{E'}\lambda(\alpha) \quad , \quad \alpha = a / R \tag{2.6.4}$$

with σ* defined in (2.6.1), are shown in Fig. 2.6.4.

	ν=0	0.1	0.2	0.3	0.4
a/R=0.15	0.0018	0.0019	0.0020	0.0020	0.022
0.2	0.0036	0.0035	0.0034	0.0033	0.0031
0.3	0.0105	0.0101	0.0097	0.0093	0.0089
0.4	0.0211	0.0202	0.0193	0.0184	0.0174
0.5	0.0346	0.0330	0.0313	0.0296	0.0277
0.6	0.0506	0.0480	0.0453	0.0424	0.0392
0.7	0.0704	0.0665	0.0624	0.0579	0.0531

Table 2.6.2 Coefficient A^*_1 according to eq.(1.2)

Constant radial tractions and disappearing tangential displacements

The internally cracked circular disk under constant radial tractions and disappearing tangential displacements along the circumference is illustrated in Fig. 2.6.4.

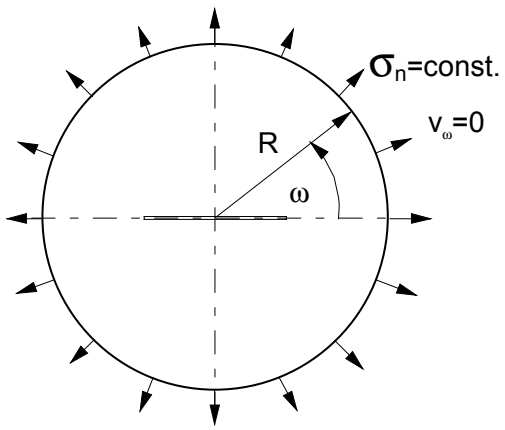

Fig. 2.6.5 Boundary conditions σ_n = constant, $v_\omega = 0$.

The stress intensity factor for the loading case of σ_n = constant, $v_\omega = 0$ is represented by eq.(2.6.1) with now σ_n instead of σ^*. The related geometric function is shown in Fig. 2.6.6a. For $\nu = 0.25$ and $a/R \le 0.7$ an approximation is given by

$$F = 1 + 0.8162\alpha^2 + 3.8905\alpha^3 - 6.3161\alpha^4 + 2.0754\alpha^5 , \quad \alpha = a / R \tag{2.6.5}$$

The T-stress is represented in Fig. 2.6.6b. A fit relation is

$$T / \sigma_n = -0.7379\alpha^2 - 7.7055\alpha^3 + 16.00\alpha^4 - 7.9212\alpha^5 \tag{2.6.6}$$

In Fig. 2.6.6 only a minor influence of ν on F and T/σ_n is visible. From the additionally introduced results for the boundary conditions of $\tau_{R\omega} = 0$ instead of $v_\omega = 0$ (see dashed curves), we find an influence of the different tangential boundary conditions only, if $\alpha > 0.4$.

The higher order coefficients A_1 and A^*_1 are compiled in Table 2.6.3 for $\nu = 0.25$.

	A_1	A^*_1
a/R=0.2	-0.1166	-0.0100
0.3	-0.0974	-0.0403
0.4	-0.0800	-0.0959
0.5	-0.0548	-0.1917
0.6	-0.0103	-0.3472
0.7	0.0706	-0.5967

Table 2.6.3 Coefficients A_1 and A^*_1 for $\nu = 0.25$ according to eq.(1.2).

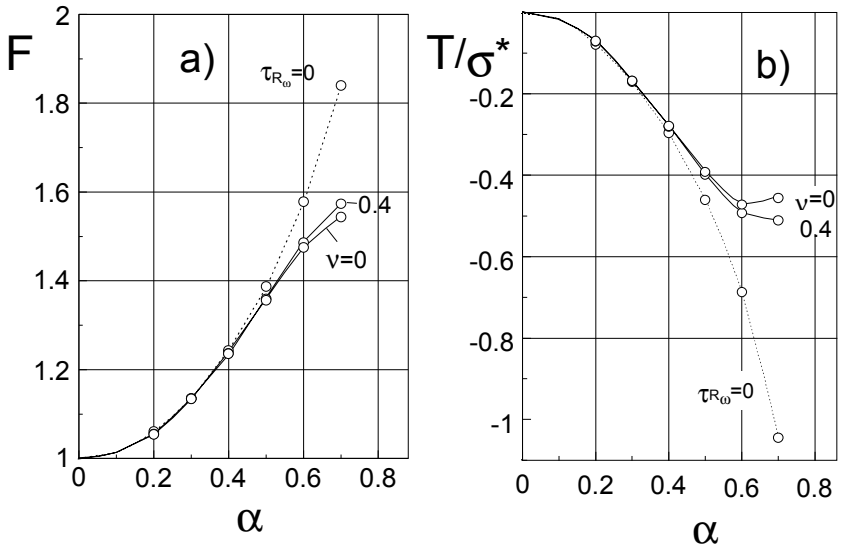

Fig. 2.6.6 Geometric function and T-stress for boundary conditions $\sigma_n = \text{constant}$, $v_\omega = 0$ (dashed curves: stress boundary conditions $\sigma_n = \text{constant}$, $\tau_{R\omega} = 0$).

2.7 Displacement boundary conditions

The internally cracked circular disk under constant radial displacement u_n and disappearing tangential displacement v_ω is shown in Fig. 2.7.1. The stress intensity factor solution, expressed by the geometric function F (see eq.(2.6.1)), is represented in Fig. 2.7.2a. The T-stress term is shown in Fig. 2.7.2b.

For $\nu = 0.25$ the results are approximated by

$$F = \tfrac{4}{3} - 2.5727\alpha^2 + 2.0487\alpha^3 + 0.9988\alpha^4 - 1.4003\alpha^5 \,, \quad \alpha = a / R \tag{2.7.1}$$

$$T / \sigma^* = 3.271\alpha^2 - 5.628\alpha^3 + 3.826\alpha^4 \tag{2.7.2}$$

The higher order coefficients A_1 and A^*_1 are compiled in Tables 2.7.1 and 2.7.2.

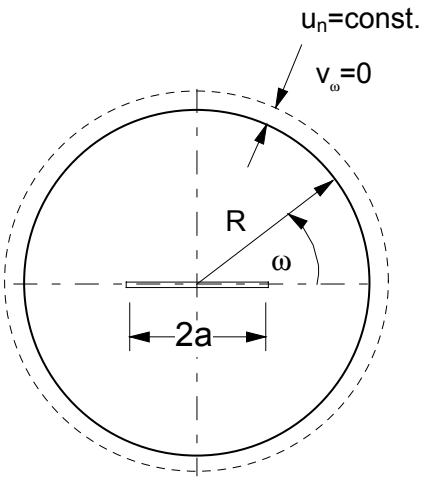

Fig. 2.7.1 Boundary conditions $u_n = u_R = \text{constant}$, $v_\omega = 0$.

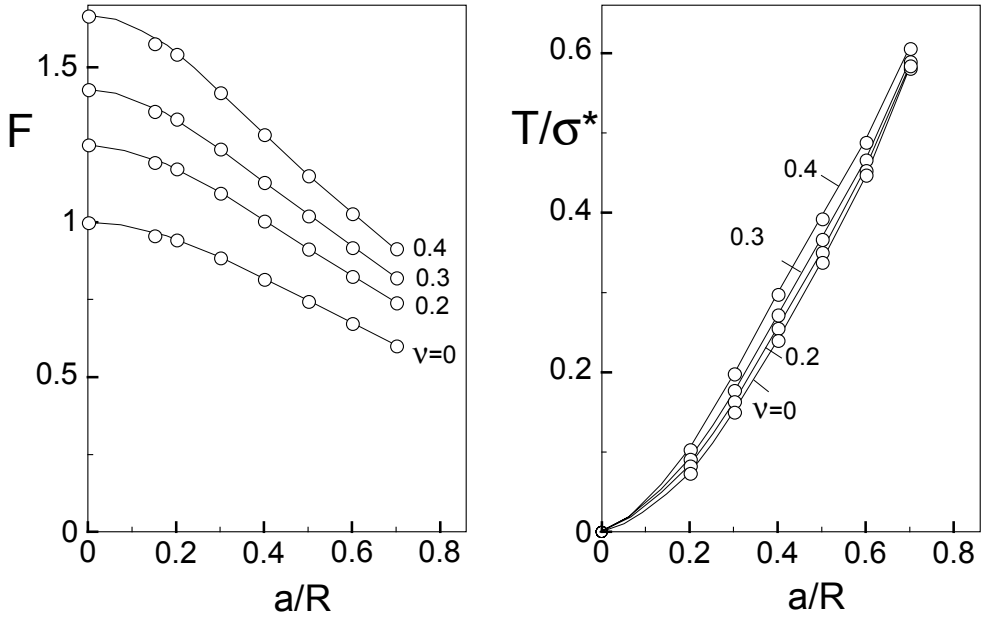

Fig. 2.7.2 Geometric function and T-stress for boundary conditions u_n = constant, $v_\omega = 0$.

	ν=0	0.2	0.3	0.4
a/R=0.2	-0.106	-0.132	-0.150	-0.174
0.3	-0.082	-0.102	-0.116	-0.133
0.4	-0.067	-0.084	-0.096	-0.110
0.5	-0.057	-0.073	-0.083	-0.095
0.6	-0.049	-0.064	-0.074	-0.085
0.7	-0.041	-0.057	-0.067	-0.079

Table 2.7.1 Coefficient A_1 according to eq.(1.2).

	ν=0	0.2	0.3	0.4
a/R=0.2	0.003	0.006	0.007	0.010
0.3	0.008	0.014	0.018	0.023
0.4	0.013	0.023	0.030	0.040
0.5	0.012	0.028	0.039	0.052
0.6	0.000	0.021	0.036	0.053
0.7	-0.040	-0.009	0.010	0.033

Table 2.7.2 Coefficient A^*_1 according to eq.(1.2).

2.8 Partially loaded disks

2.8.1 Stress boundary conditions

The case of different stress boundary conditions over parts of the circumference is dealt within Section 2.2. Results for the stress intensity factor K are expressed by the geometric function F according to

$$K = \sigma_n \sqrt{\pi a} F(\gamma, a / R) \tag{2.8.1}$$

and represented in Fig. 2.8.1.

The T-stresses are illustrated in Fig. 2.8.2 as a function of the loading angle γ and the crack size a/R.

In Tables 2.8.1 and 2.8.2 the next higher order coefficients of the stress function, eq.(1.2), are given.

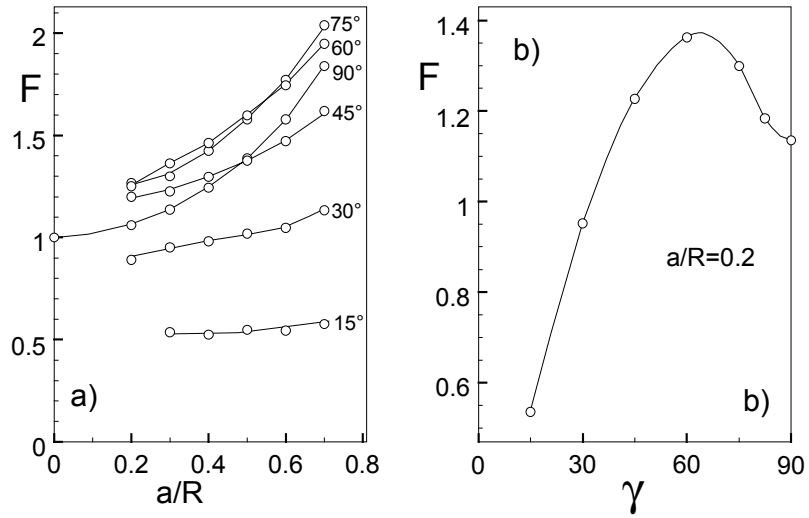

Fig. 2.8.1 Geometric function F according to eq.(6.6.1)

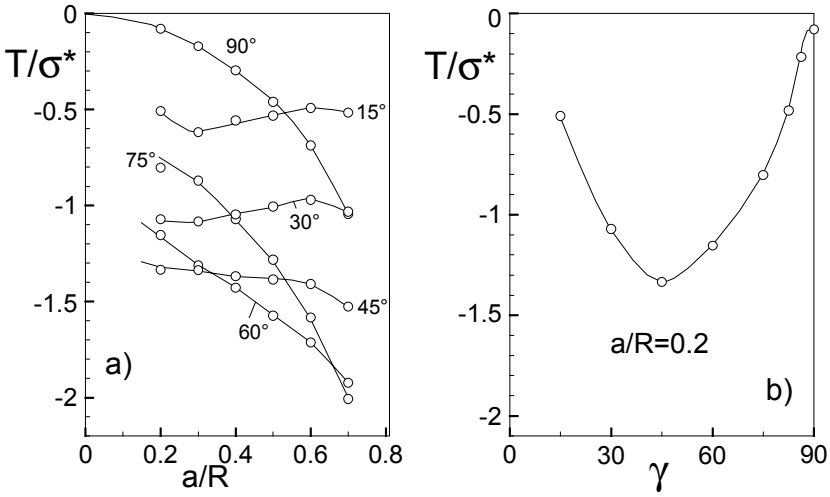

Fig. 2.8.2 T-stress as a function of crack size and loading angle γ.

	A_1	A^*_1
a/R=0.2	-0.115	-0.1659
0.3	-0.0766	-0.2554
0.4	-0.0393	-0.3977
0.5	0.0056	-0.5672
0.6	0.0598	-0.7338
0.7	0.1344	-0.9290

Table 2.8.1 Coefficients A_1 and A^*_1 according to eq.(1.2) for $\gamma = 45°$.

	A_1	A^*_1
a/R = 0.2	-0.117	-0.0116
0.3	-0.0979	-0.0359
0.4	-0.0828	-0.0796
0.5	-0.0640	-0.1465
0.6	-0.0346	-0.2473
0.7	0.0179	-0.4107

Table 2.8.2 Coefficients A_1 and A^*_1 according to eq.(1.2) for $\gamma = 90°$.

2.8.2 Mixed boundary conditions in the loading region

An internally cracked circular disk with constant radial displacements u_R over the angle 2γ and disappearing normal tractions σ_n on the remaining part of the surface is shown in Fig. 2.8.3. In this loading case the shear tractions along the circumference were chosen to be $\tau_{R\omega} = 0$.

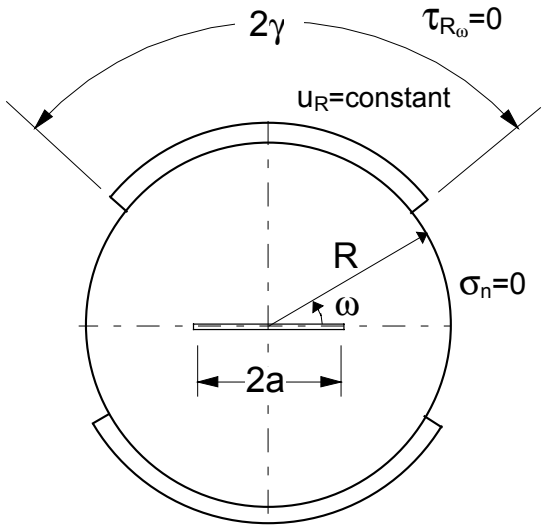

Fig. 2.8.3 Partially loaded, internally cracked disk under mixed boundary conditions: constant radial displacement over angle 2γ, disappearing normal tractions elsewhere, disappearing shear tractions along the whole circumference.

The stress intensity factor for the loading case of u_R = constant, $\tau_{R\omega} = 0$ is defined by

$$K = \sigma^* \sqrt{\pi a}\, F(a / R, \nu, \gamma) \ , \quad \sigma^* = \frac{u_R E}{R} \tag{2.8.1}$$

(E= Young's modulus, F = geometric function). Results of the Boundary Collocation computations are represented in Fig. 2.8.4 for a Poisson's ratio of ν = 0.25 and several loading angles γ. The influence of the Poisson's ratio is shown in Fig. 2.8.5. The T-stress is represented in Fig. 2.8.6.

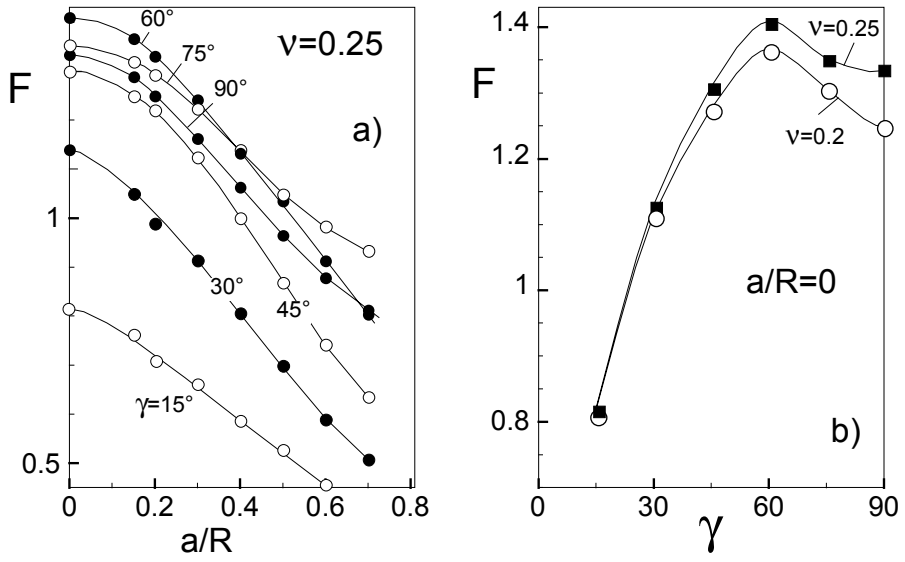

Fig. 2.8.4 Geometric function F, defined by eq.(2.8.1), as a function of crack size and loading angle.

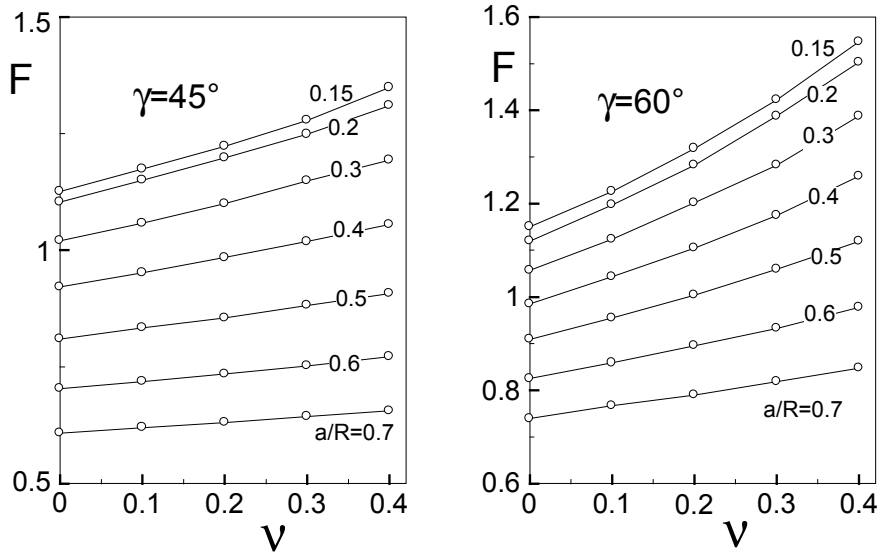

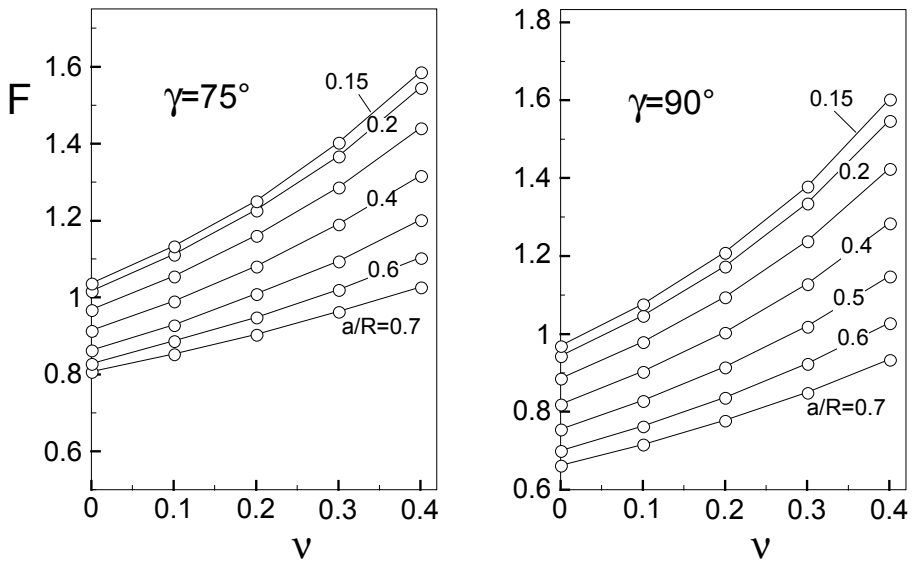

Fig. 2.8.5 Influence of the Poisson's ratio ν on the geometric function *F*.

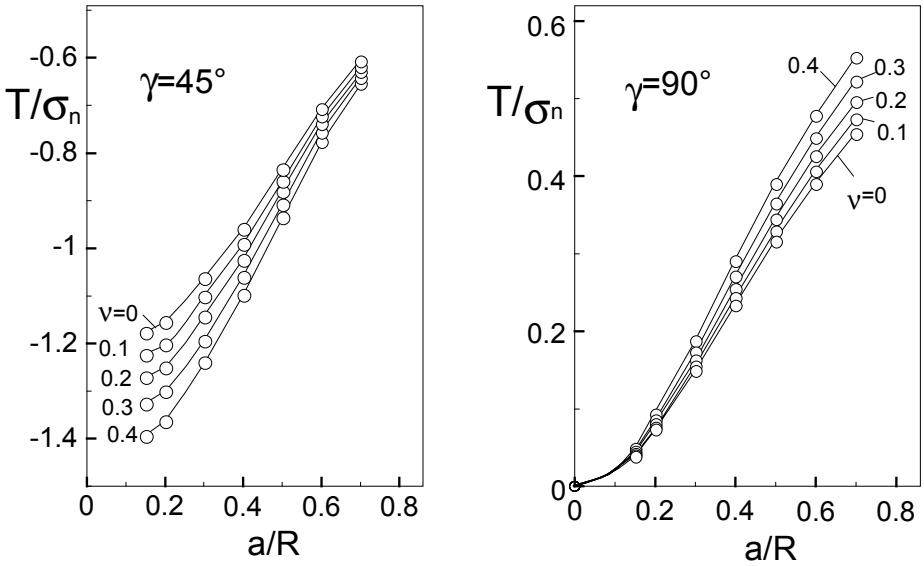

Fig. 2.8.6 T-stress as a function of crack size, Poisson's ratio, and loading angle γ.

2.8.3 Displacement boundary conditions in the loading region

The internally cracked circular disk with constant radial displacements u_R and disappearing tangential displacements v_ω over the angle 2γ and traction free surfaces elsewhere is shown in Fig. 2.8.7.

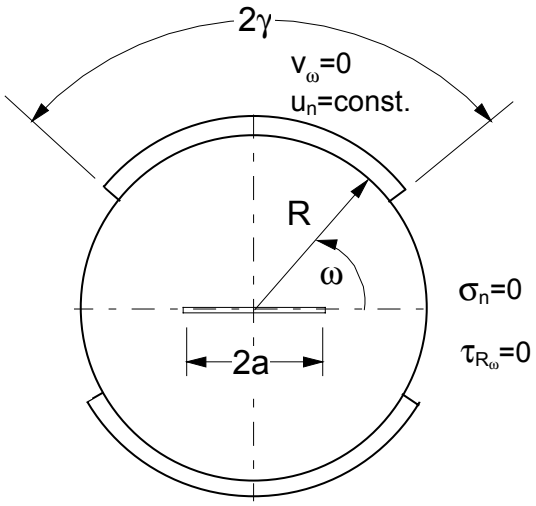

Fig. 2.8.7 Partially loaded, internally cracked disk under mixed boundary conditions: constant radial and disappearing tangential displacements over angle 2γ, disappearing tractions elsewhere.

The geometric function according to eq.(2.8.1) is plotted in Fig. 2.8.8 as a function of γ, a/R, and ν. The T-stress is shown in Fig. 2.8.9.

In Fig. 2.8.10 the geometric function and the T-stresses are plotted for the two boundary conditions in the loading region: u_R = constant, v_ω =0 (solid curves) and u_R = constant, $\tau_{R\omega} = 0$ (dashed curves). Only very small differences can be detected.

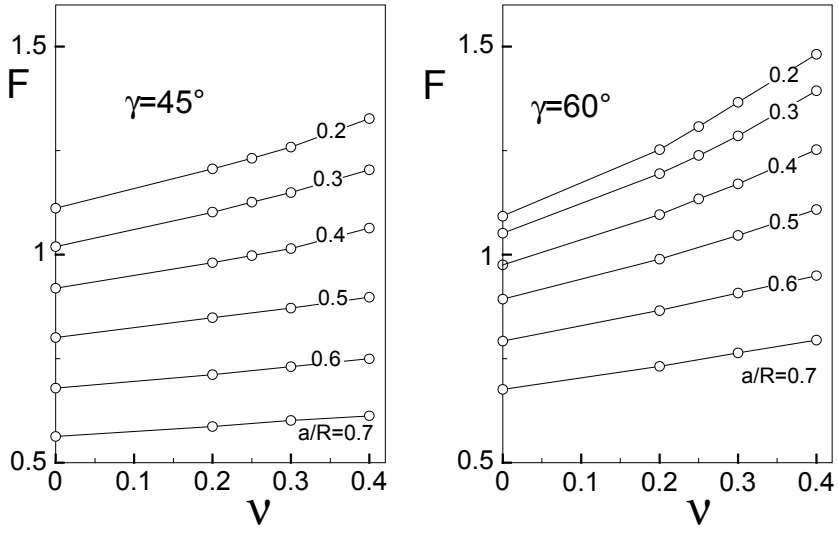

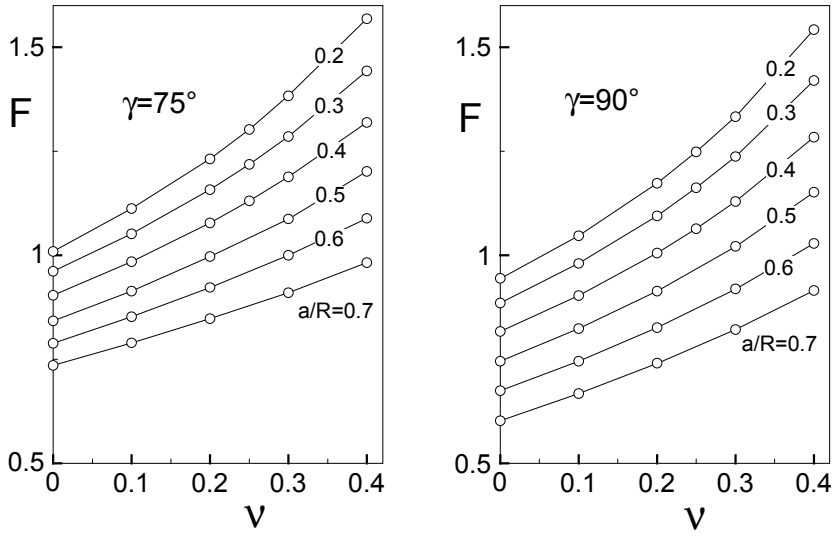

Fig. 2.8.8 Influence of the Poisson's ratio ν on the geometric function *F*.

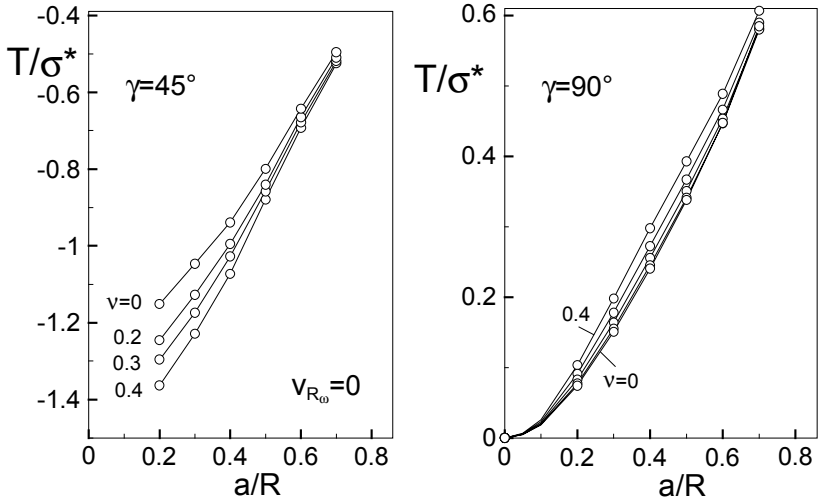

Fig. 2.8.9 T-stress as a function of crack size, Poisson's ratio, and loading angle γ.

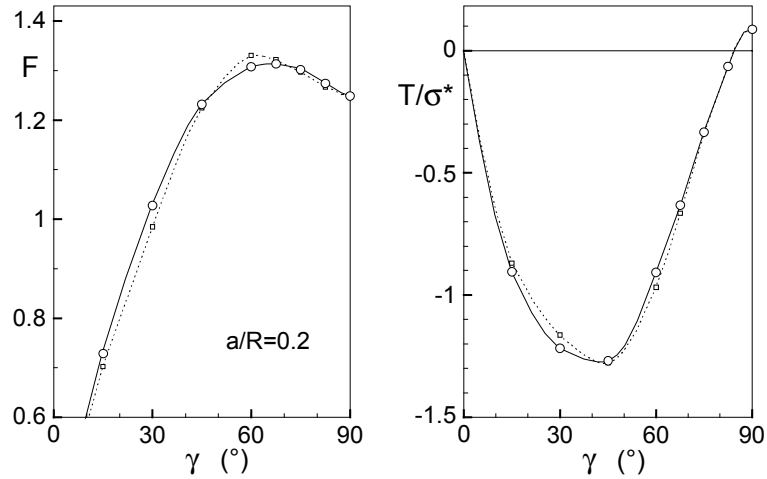

Fig. 2.8.10 Influence of the tangential boundary condition in the loading range on *F* and T-stress. Solid curve u_R=const., v_ω=0; dashed curve: u_R=const., $\tau_{R\omega}$=0.

3 Edge-cracked circular disk

Edge-cracked circular disks are often used as fracture mechanics test specimens. Figure 3.1 shows the geometric data.

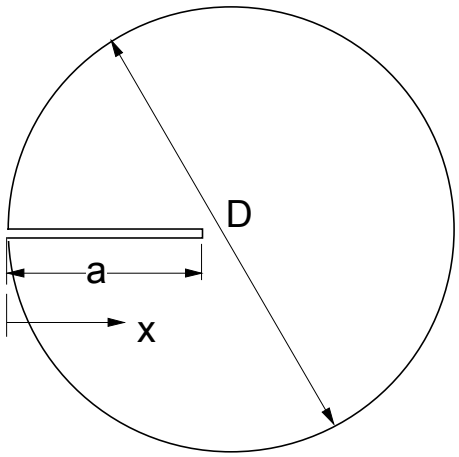

Fig. 3.1 Geometric data of an edge-cracked circular disk.

3.1 Circumferentially loaded disk (traction boundary conditions)

A circular disk is loaded by constant normal tractions σ_n along the circumference (for loading see Fig. 3.1.1)

$$\sigma_n = \sigma_R = \text{const}\,, \quad \tau_{R\omega} = 0 \tag{3.1.1}$$

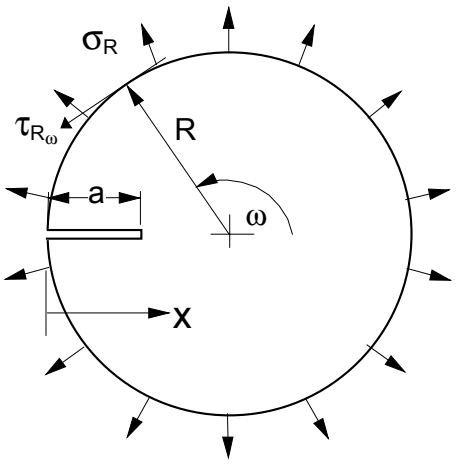

Fig. 3.1.1 Edge-cracked circular disk under pure stress boundary conditions.

The stress intensity factor solution is for this loading case

$$K_I = \sigma_n F \sqrt{\pi a}\,, \quad F = \frac{1.1215}{(1-\alpha)^{3/2}}, \quad \alpha = a / D \tag{3.1.2}$$

For a single-edge-cracked disk a weight function is given in [6]

$$h(x,a)=\sqrt{\frac{2}{\pi a}}\left[\frac{\rho}{\sqrt{1-\rho}}+D_0\sqrt{1-\rho}+D_1(1-\rho)^{3/2}+D_2(1-\rho)^{5/2}\right] \tag{3.1.3}$$

with the coefficients

$$\begin{aligned}D_0&=(1.5721+2.4109\,\alpha-0.8968\,\alpha^2-1.4311\,\alpha^3)/(1-\alpha)^{3/2}\\ D_1&=(0.4612+0.5972\,\alpha+0.7466\,\alpha^2+2.2131\,\alpha^3)/(1-\alpha)^{3/2}\\ D_2&=(-0.2537+0.4353\,\alpha-0.2851\,\alpha^2-0.5853\,\alpha^3)/(1-\alpha)^{3/2}\end{aligned}$$

In this case it holds [6]

$$A^*_0\,(1-\alpha)^2=-0.11851=C^*_0 \tag{3.1.4}$$

and, from eqs.(1.14) and (1.26)

$$\begin{aligned}\frac{T}{\sigma_n}&=-4A^*_0=\frac{0.474}{(1-\alpha)^2}\\ \frac{T_c}{\sigma_n}&=\frac{0.474}{(1-\alpha)^2}-1\end{aligned} \tag{3.1.5}$$

The value C^*_0 occurring in eq.(3.1.4) is identical with the coefficient of Wigglesworth's [25] expansion for the edge-cracked semi-infinite body.
The biaxiality ratio results as

$$\beta=\frac{0.4227}{\sqrt{1-\alpha}} \tag{3.1.6}$$

Using eq.(3.1.5) as the reference T-stress solution, the coefficient C for the Green's function, represented by eq.(1.28), follows as

$$C=\frac{0.9481}{a(1-\alpha)^2},\quad \alpha=a/D \tag{3.1.7}$$

Consequently, the T-stress can be computed from

$$T=\frac{0.9481}{(1-\alpha)^2}\int_0^1(1-\rho)\,\sigma_y(\rho)\,d\rho-\sigma_y\big|_{x=a},\quad \rho=x/a \tag{3.1.8}$$

Further coefficients of the Williams stress function are [7]

$$A_1=\frac{-0.02279+0.1322\,\alpha}{(1-\alpha)^{5/2}\sqrt{\alpha}} \tag{3.1.9}$$

$$A^*_1 = \frac{0.04812 - 0.1185\alpha}{(1-\alpha)^3\alpha} \tag{3.1.10}$$

$$A_2 = \frac{-0.00680 - 0.03416\alpha + 0.0991\alpha^2}{(1-\alpha)^{7/2}\alpha^{3/2}} \tag{3.1.11}$$

$$A^*_2 = \frac{-0.01787 + 0.09627\alpha - 0.11851\alpha^2}{(1-\alpha)^4\alpha^2} \tag{3.1.12}$$

For special applications also crack opening displacements δ at the crack mouth $x = 0$ are of interest. Figure 3.1.2 represents the displacements under constant normal tractions σ_n in the form

$$\delta = \frac{2a\sigma_n}{E'}(1 - a/D)^2\ \lambda(a/D) \tag{3.1.13}$$

The results of boundary collocation computations are represented by the circles. From a least-squares fit we obtain the representation

$$\lambda = 1.454 + 0.526\, a/D \tag{3.1.14}$$

The dashed curve in Fig. 3.1.2 is the solution for the single edge-cracked endless parallel strip as reported by Tada [1].

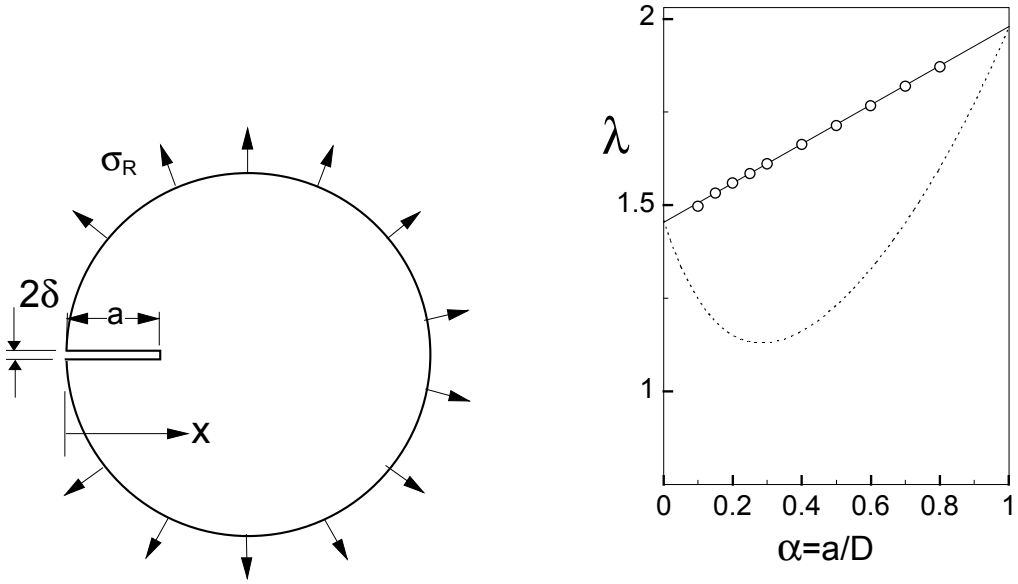

Fig. 3.1.2 Crack-mouth displacements ($x = 0$) according to eq.(3.1.13); circles: edge-cracked disk, dashed curve: results for the single edge-cracked endless parallel strip, reported by Tada [1].

The stress intensity factor for mode-II loading by constant shear tractions τ_0 is

$$K_{II} = \tau_0 F_{II} \sqrt{\pi a} \tag{3.1.15}$$

The related geometric function F_{II} is plotted in Fig. 3.1.3. A fit relation for $\alpha = a/2R \le 0.8$ is given by eq.(3.1.16).

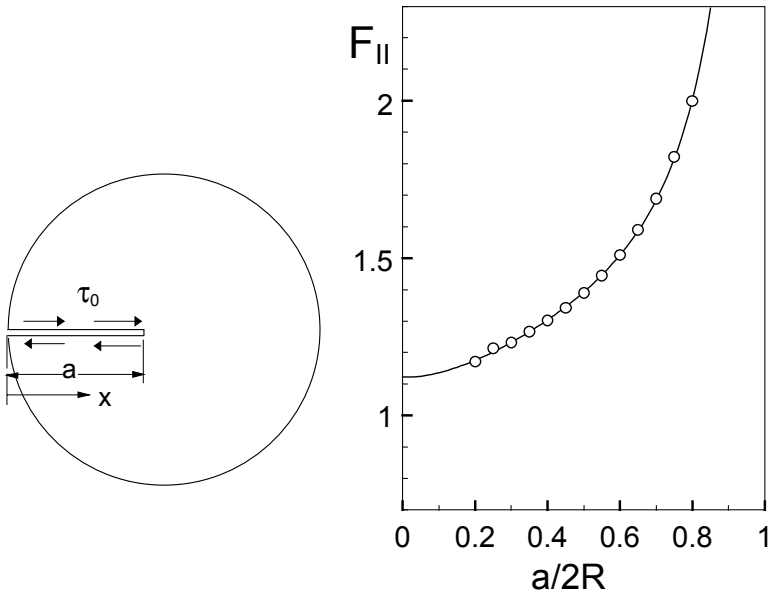

Fig. 3.1.3 Geometric function for loading by constant shear tractions on the crack faces.

$$F_{II} = \frac{1.1216 - 0.5608\,\alpha + 1.3433\,\alpha^2 - 1.9734\,\alpha^3 + 0.8954\,\alpha^4}{\sqrt{1-\alpha}} \tag{3.1.16}$$

A mode-II weight function is

$$h_{II}(x,a) = \sqrt{\frac{2}{\pi a}}\left[\frac{1}{\sqrt{1-\rho}} + D_0\sqrt{1-\rho} + D_1(1-\rho)^{3/2} + D_2(1-\rho)^{5/2}\right] \tag{3.1.17}$$

with coefficients compiled in Table 3.1.1, which can be interpolated by cubic splines.

For $a/2R \le 0.55$ the coefficients are approximated by

$$D_0 = \frac{0.407 + 0.2393\,\alpha + 4.6661\,\alpha^2 - 0.547\,\alpha^3}{(1-\alpha)^{3/2}} \tag{3.1.18}$$

$$D_1 \cong 0.70 \tag{3.1.19}$$

$$D_2 \cong -0.3092 + 0.0202\,\alpha + 0.1913\,\alpha^2 \tag{3.1.20}$$

Higher order coefficients for the antisymmetric stress function, eq.(1.2'), are compiled in Table 3.1.2.

a/2R	D_0	D_1	D_2
0.1	0.4981	0.6931	-0.305
0.2	0.6228	0.6853	-0.296
0.25	0.7069	0.6856	-0.290
0.3	0.8032	0.6896	-0.284
0.35	0.9118	0.6965	-0.278
0.4	1.034	0.7044	-0.272
0.45	1.172	0.7096	-0.264
0.5	1.332	0.7064	-0.253
0.55	1.523	0.6861	-0.236
0.6	1.759	0.6352	-0.210
0.65	2.062	0.5321	-0.169
0.7	2.470	0.3394	-0.103
0.75	3.052	-0.013	0.006
0.8	3.944	-0.674	0.198

Table 3.1.1 Coefficients for the mode-II weight function eq.(3.1.17).

a/2R	B^*_0	B_1	B^*_1
0.2	0.175	0.217	-0.832
0.3	0.164	0.144	-0.441
0.4	0.178	0.089	-0.276
0.5	0.215	0.039	-0.159
0.6	0.294	-0.018	0.000
0.7	0.471	-0.094	0.412
0.8	0.981	-0.229	2.231

Table 3.1.2 Higher order coefficients according to eq.(1.2') for mode-II loading.

3.2 Diametrically loaded disk

3.2.1 Load perpendicular to the crack

A disk of unit thickness is considered, which is diametrically loaded by a pair of forces P (Fig. 3.2.1). The forces may act perpendicularly to the crack plane. In this case the stresses are given by

$$\frac{\sigma_y}{\sigma^*} = \frac{4}{[1+(1-\xi)^2]^2} - 1\,, \quad \xi = x\,/\,R\,,\; R = D\,/\,2 \tag{3.2.1}$$

$$\frac{\sigma_x}{\sigma^*} = \frac{4(1-\xi)^2}{[1+(1-\xi)^2]^2} - 1\,, \quad \sigma^* = \frac{P}{\pi R t} \tag{3.2.2}$$

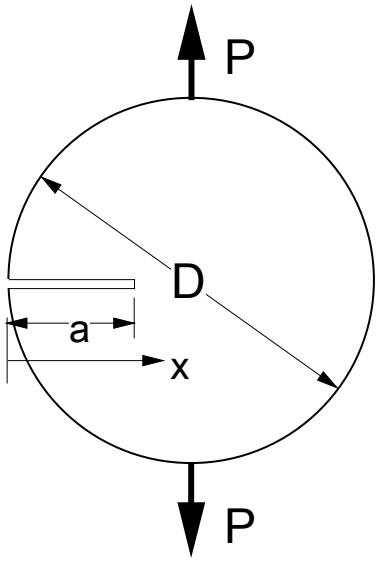

Fig. 3.2.1 Diametrically loaded circular disk.

The stress intensity factor results from eq.(1.19a) with the weight function of eq.(3.1.3) and the T-term from eq.(3.1.8)

$$T_c \cong \frac{0.9481\sigma^*}{2(1-\alpha)^2(a\,/\,R)^2}\left[4\left(1-\frac{a}{R}\right)\arctan\left(1-\frac{a}{R}\right)+2\frac{a}{R}-\frac{a^2}{R^2}-\pi\left(1-\frac{a}{R}\right)\right]-\sigma_y\big|_{x=a} \tag{3.2.3}$$

Considering the total x-stress (crack contribution and x-stress component in the uncracked body), the biaxiality ratio can be computed according to eq.(1.17). The T-stress and the stress intensity factor result in the biaxiality ratio β which is shown as a curve in Fig. 3.2.2.

In addition to the Green's function computations, the biaxiality ratios were directly determined with the Boundary Collocation method (BCM) which provides the coefficients A_0, A^*_0 and by eq.(1.18) the quantity β for diametrical loading. The results are entered as circles. An excellent agreement is obvious between the BCM results and those obtained from the Green's function representation. This is an indication of an adequate description of the Green's function by the set-up eq.(1.28) using one regular term only.

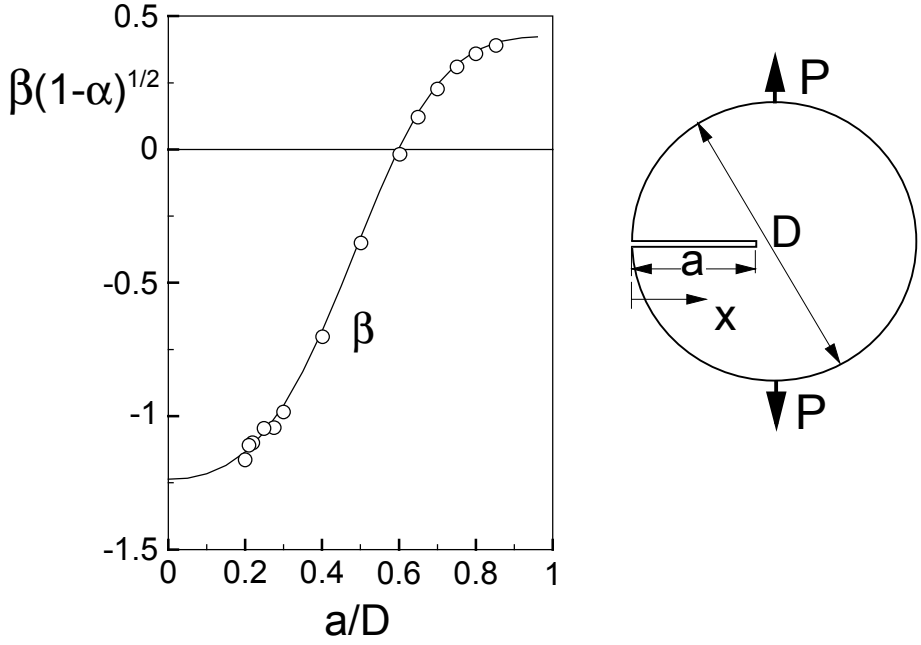

Fig. 3.2.2 Biaxiality ratio for an edge-cracked circular disk diametrically loaded by a pair of forces; line: eq.(3.2.6), circles: BCM results.

a/D	$T(1-a/D)^2$	$\beta(1-a/D)^{1/2}$
0	0	-1.236
0.1	-0.364	-1.216
0.2	-0.732	-1.134
0.3	-0.970	-0.960
0.4	-0.915	-0.682
0.5	-0.526	-0.333
0.6	0.007	0.004
0.7	0.430	0.245
0.8	0.652	0.370

Table 3.2.1 T-stress and biaxiality ratio for diametral point forces.

3.3 Circumferentially loaded disk under mixed boundary conditions

Edge-cracked circular disks under mixed boundary conditions are shown in Fig. 3.3.1.

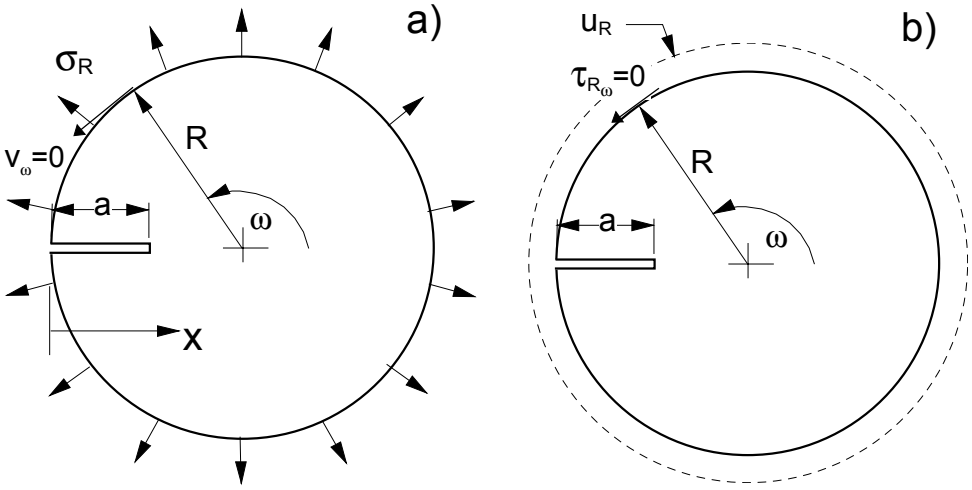

Fig. 3.3.1 Edge-cracked disk under mixed boundary conditions; a) constant normal tractions, disappearing circumferential displacements, b) constant radial displacement, disappearing shear tractions at the surface.

Case: $u_R = \text{constant}$, $\tau_{R\omega}=0$

With the scaling stress

$$\sigma^* = \frac{u_R E}{R} \tag{3.3.1}$$

the stress intensity factor is

$$K_I = \sigma^* \sqrt{\pi a}\, F(a/2R, \nu) \tag{3.3.2}$$

with the geometric function F plotted in Fig. 3.3.2a for several Poisson's ratios. For the special value of $\nu = 0.25$ the results are fitted as

$$F = \tfrac{4}{3} + 0.953\,\alpha + 20.157\,\alpha^2 - 107.35\,\alpha^3 + 156.09\,\alpha^4 - 72.69\,\alpha^5 \tag{3.3.3}$$

Using a modified geometric function

$$F^* = (1-\nu)F \tag{3.3.4}$$

a coincidence of the curves is visible for $a/2R \to 0$ (see Fig. 3.3.2b).
The T-stresses are shown in Fig. 3.3.3. An approximation for $\nu = 0.25$ and $\alpha = a/2R \le 0.75$ is

$$T/\sigma^* = -3.137\,\alpha^2 + 40.744\,\alpha^3 - 76.904\,\alpha^4 + 41.623\,\alpha^5 \tag{3.3.5}$$

The higher order coefficients of eq.(1.2) are compiled in Tables 3.3.1 and 3.3.2.

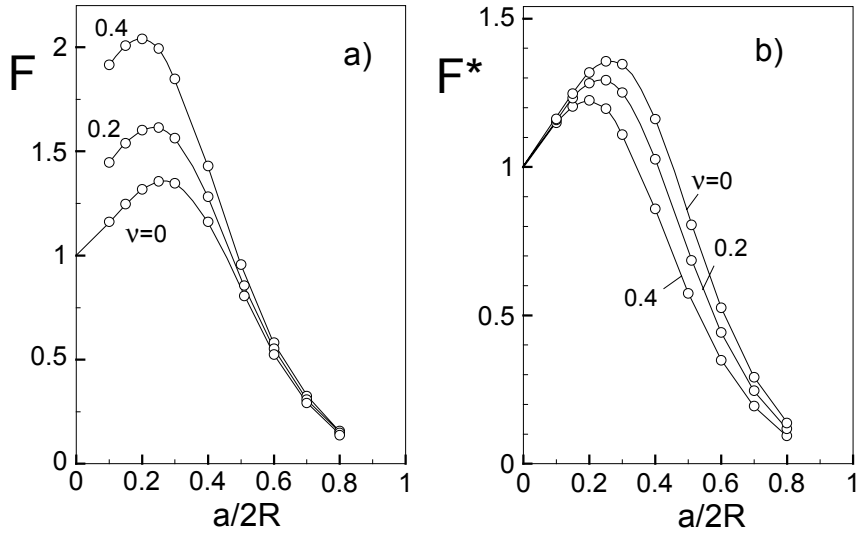

Fig. 3.3.2 Stress intensity factor for the boundary conditions of u_R = constant, $\tau_{R\omega} = 0$. For F see eq.(3.3.2) and for F^* eq.(3.3.4).

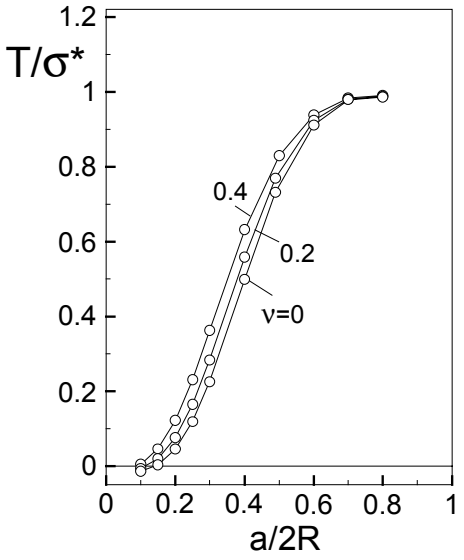

Fig. 3.3.3 T-stress for **the** boundary conditions of u_R = constant, $\tau_{R\omega} = 0$.

a/2R	ν=0	0.2	0.4
0.1	-0.0983	-0.1209	-0.158
0.2	-0.0389	-0.0450	-0.0546
0.3	0.0189	0.0239	0.0305
0.4	0.0721	0.0802	0.0901
0.5	0.1035	0.110	0.1166
0.6	0.1113	0.1153	0.1196
0.7	0.1036	0.1072	0.1108
0.8	0.0879	0.0920	0.0960

Table 3.3.1 Coefficient A_1 according to eq.(1.2).

a/2R	ν=0	0.2	0.4
0.1	0		
0.2	0	0	
0.3	0	0	
0.4	0.001	0	0
0.5	0.007	0.006	0.005
0.6	0.017	0.013	0.010
0.7	0.030	0.024	0.017
0.8	0.047	0.037	0.027

Table 3.3.2 Coefficient A^*_1 according to eq.(1.2).

Figure 3.3.4 represents the crack opening displacements δ (for δ see Fig. 3.1.2) under constant radial displacements and disappearing shear tractions at the circumference in the form

$$\delta = \frac{2a\sigma^*}{E'}\lambda(a/D) \tag{3.3.6}$$

with σ* given by eq.(3.3.1).

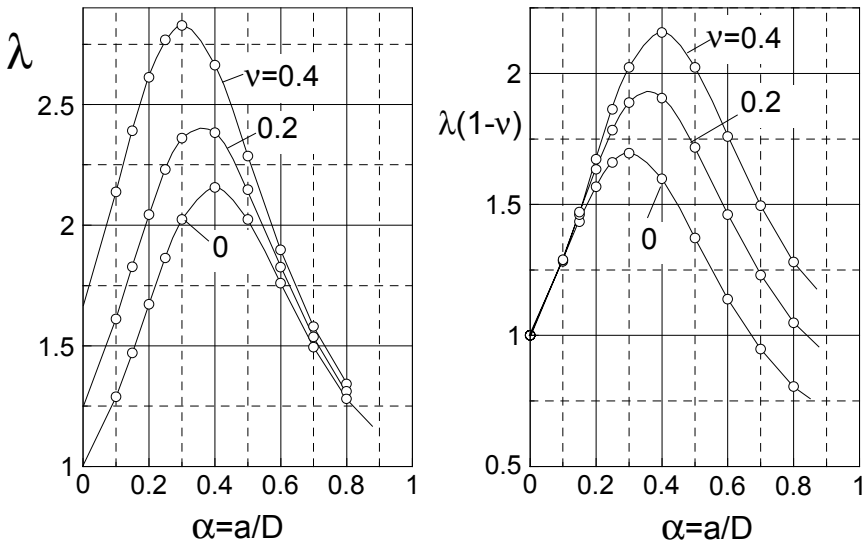

Fig. 3.3.4 Crack-mouth displacement represented by eq.(3.3.6). Boundary conditions: u_R = constant, $\tau_{R\omega} = 0$.

Case: σ_R = constant, $v_R = 0$

In this case the stress intensity factor is

$$K_I = \sigma_R\sqrt{\pi a}\,F(a/2R,\nu) \tag{3.3.7}$$

The geometric function is plotted in Fig. 3.3.5a for several values of ν. Figure 3.3.5b represents the T-stress. For the special value of ν = 0.25 the geometric function is fitted as

$$F = 0.6163 + 0.2603\alpha + 0.6739\alpha^2 - 0.4497\alpha^3 \qquad (3.3.7)$$

The higher order coefficients A_1 and A^*_1 of eq.(1.2) are compiled in Tables 3.3.3 and 3.3.4.

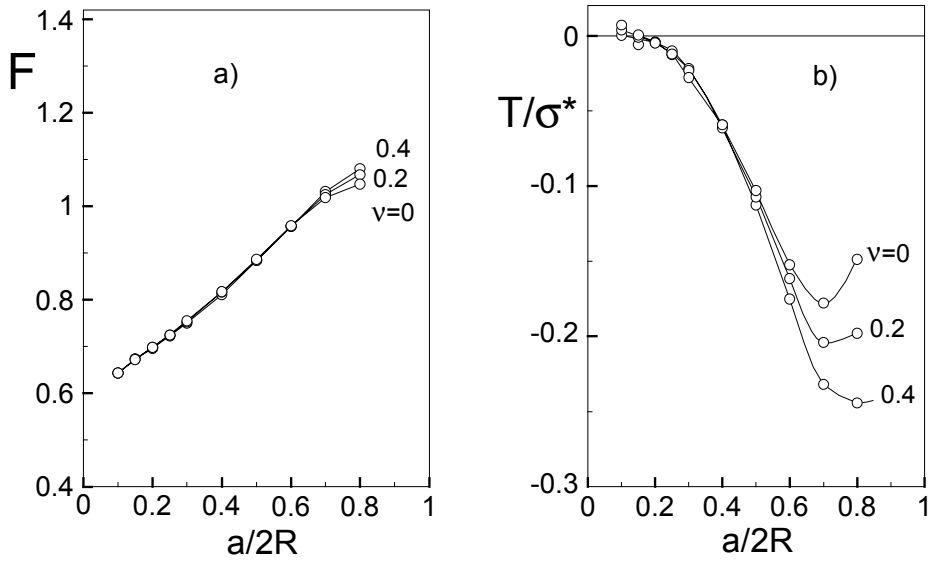

Fig. 3.3.5 Geometric function and T-stress for the boundary conditions of σ_n = constant, $\nu_R = 0$.

a/2R	ν=0	0.2	0.4
0.1	-0.176	-0.176	-0.176
0.2	-0.124	-0.123	-0.122
0.3	-0.100	-0.099	-0.098
0.4	-0.080	-0.080	-0.080
0.5	-0.058	-0.059	-0.061
0.6	-0.029	-0.031	-0.034
0.7	0.018	0.013	0.009
0.8	0.100	0.096	0.088

Table 3.3.3 Coefficient A_1 according to eq.(1.2).

a/2R	ν=0	0.2	0.4
0.1	0.047	0.040	0.024
0.2	-0.059	-0.067	-0.078
0.3	-0.087	-0.092	-0.095
0.4	-0.130	-0.130	-0.129
0.5	-0.191	-0.186	-0.181
0.6	-0.281	-0.270	-0.260
0.7	-0.420	-0.405	-0.392
0.8	-0.664	-0.657	-0.626

Table 3.3.4 Coefficient A^*_1 according to eq.(1.2).

3.4 Disk under displacement boundary conditions

An edge-cracked circular disk under pure displacement boundary conditions is shown in Fig. 3.4.1.

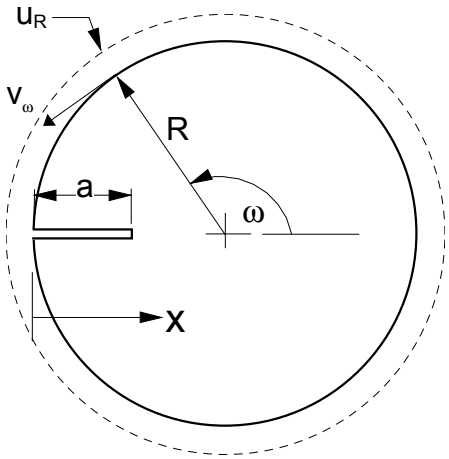

Fig. 3.4.1 Edge-cracked disk under pure displacement boundary conditions: constant radial displacement, disappearing tangential displacements.

Case: u_R = constant, $\tau_{R\omega}$=0

With the scaling stress given by eq.(3.3.1), the stress intensity factor is

$$K_I = \sigma^* \sqrt{\pi a}\, F(a/2R, \nu) \tag{3.4.1}$$

with the geometric function F plotted in Fig. 3.4.2 for several Poisson's ratios. The T-stresses are shown in Fig. 3.4.3.

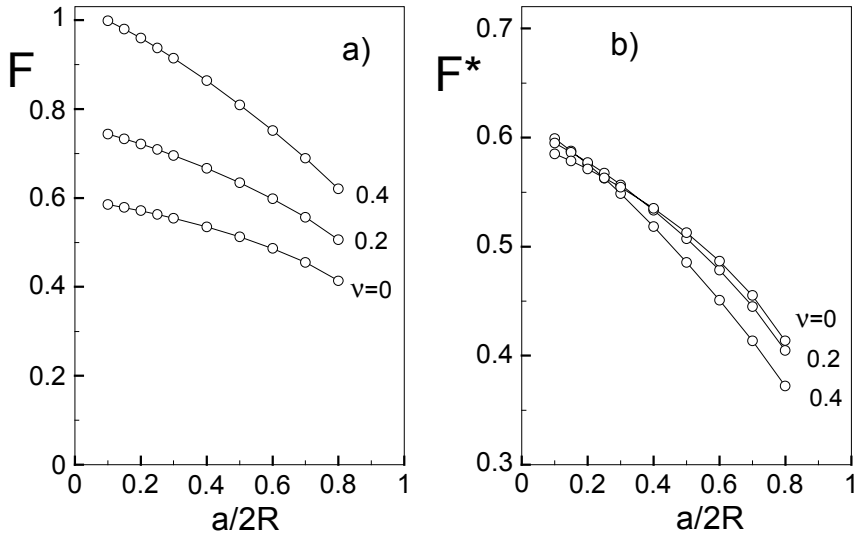

Fig. 3.4.2 Geometric functions for the boundary conditions of u_R = constant, $v_R = 0$. For F see eq.(3.4.1), for F^* eq.(3.3.4).

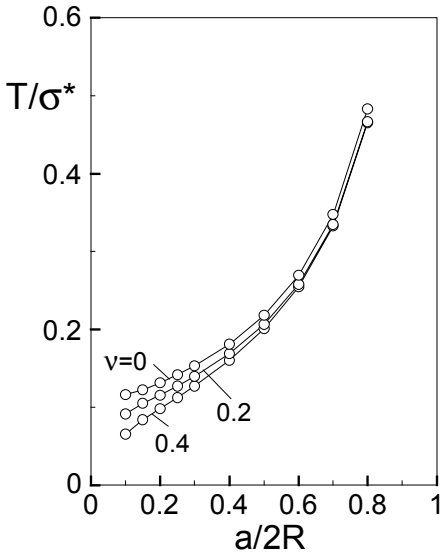

Fig. 3.4.3 T-stress for the boundary conditions of u_R = constant, $v_R = 0$.

For the special value $\nu = 0.25$ the results are fitted as

$$F = 0.814 - 0.175\,\alpha - 0.2192\,\alpha^2 \tag{3.4.2}$$

and the related T-stress (for $0.1 \le a/2R \le 0.8$) by

$$T / \sigma^* = 0.0388 + 0.5568\,\alpha - 1.1934\,\alpha^2 + 1.448\,\alpha \tag{3.4.3}$$

The higher order coefficients of eq.(1.2) are compiled in Tables 3.4.1 and 3.4.2.

a/2R	ν=0	0.2	0.4
0.1	-0.171	-0.213	-0.283
0.2	-0.120	-0.149	-0.197
0.3	-0.097	-0.120	-0.157
0.4	-0.083	-0.102	-0.133
0.5	-0.073	-0.090	-0.115
0.6	-0.064	-0.080	-0.102
0.7	-0.057	-0.071	-0.091
0.8	-0.047	-0.062	-0.082

Table 3.4.1 Coefficient A_1 according to eq.(1.2).

a/2R	ν=0	0.2	0.4
0.1	0.257	0.248	0.260
0.2	0.136	0.142	0.159
0.3	0.099	0.107	0.125
0.4	0.082	0.090	0.108
0.5	0.071	0.080	0.098
0.6	0.061	0.073	0.092
0.7	0.048	0.063	0.085
0.8	0.014	0.037	0.067

Table 3.4.2 Coefficient A^*_1 according to eq.(1.2).

3.5 Brazilian disk (edge-cracked)

The diametral compression test (Brazilian disk test) is illustrated in Fig. 3.5.1.

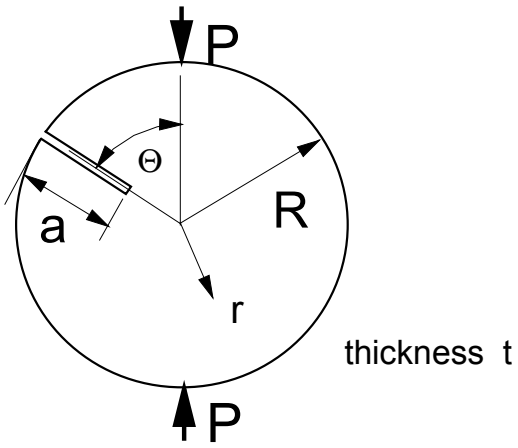

Fig. 3.5.1 Brazilian disk test with edge-cracked disk.

The circumferential and radial stress components in an uncracked Brazilian disk have been given by Erdlac (quoted in [19]) as

$$\sigma_\varphi = \sigma_n = \frac{2P}{\pi t R}\left[\frac{1}{2} - \frac{(1-\rho\cos\Theta)\sin^2\Theta}{(1+\rho^2-2\rho\cos\Theta)^2} - \frac{(1+\rho\cos\Theta)\sin^2\Theta}{(1+\rho^2+2\rho\cos\Theta)^2}\right], \quad \rho = r/R \tag{3.5.1}$$

$$\sigma_r = \frac{2P}{\pi t R}\left[\frac{1}{2} - \frac{(1-\rho\cos\Theta)(\cos\Theta-\rho)^2}{(1+\rho^2-2\rho\cos\Theta)^2} - \frac{(1+\rho\cos\Theta)(\cos\Theta+\rho)^2}{(1+\rho^2+2\rho\cos\Theta)^2}\right] \tag{3.5.2}$$

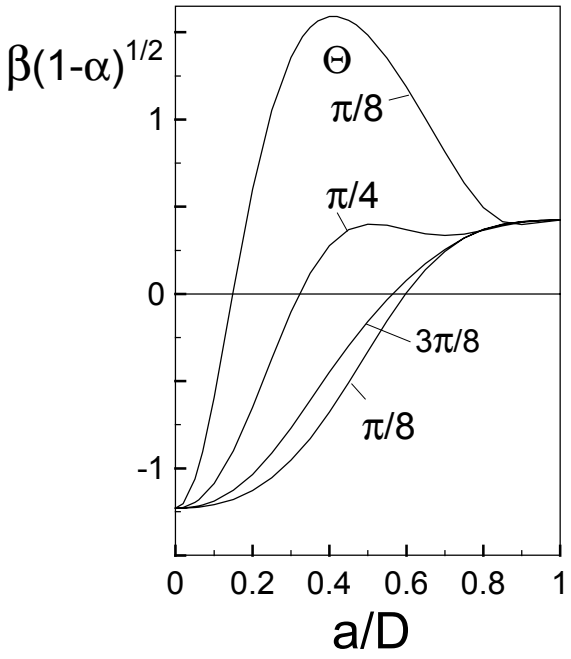

Fig. 3.5.2 Brazilian disk test with an edge-cracked disk and biaxiality ratio $\beta(1-\alpha)^{1/2}$, $\alpha = a/D$.

Using eq.(3.1.8) the T-stress can be determined. The T-stress term, evaluated for several relative crack depths a/W and several angles Θ, is compiled in Tables 3.5.1 and 3.5.2 and the biaxiality ratio in Table 3.5.3.

$\alpha = a/2R$	$\Theta = \pi/16$	$\pi/8$	$\pi/4$	$3\pi/8$	$7\pi/16$	$\pi/2$
0	0	0	0	0	0	0
0.05	2.671	1.086	0.359	0.215	0.191	0.184
0.1	0.933	1.466	0.715	0.460	0.415	0.401
0.2	-1.687	0.194	1.068	0.979	0.937	0.922
0.3	-2.319	-1.099	0.691	1.328	1.428	1.456
0.4	-2.546	-1.824	-0.078	1.235	1.577	1.691
0.5	-2.744	-2.310	-0.896	0.518	0.952	1.104
0.6	-3.050	-2.814	-1.906	-1.153	-0.959	-0.894
0.65	-3.290	-3.163	-2.727	-2.637	-2.662	-2.675
0.7	-3.637	-3.683	-4.085	-4.911	-5.196	-5.297

Table 3.5.1 T-stress T_c/σ^* for the Brazilian disk test ($\sigma^*=P/(\pi Rt)$).

$\alpha = a/2R$	$\Theta = \pi/16$	$\pi/8$	$\pi/4$	$3\pi/8$	$7\pi/16$	$\pi/2$
0	0.000	0.000	0.000	0.000	0.000	0.000
0.05	1.858	1.067	0.376	0.227	0.203	0.195
0.1	-1.979	1.097	0.760	0.511	0.464	0.449
0.15	-4.587	-0.044	1.015	0.837	0.784	0.766
0.2	-5.482	-1.470	1.020	1.172	1.152	1.143
0.25	-5.669	-2.610	0.743	1.467	1.543	1.561
0.3	-5.633	-3.383	0.252	1.670	1.910	1.981
0.35	-5.556	-3.888	-0.337	1.737	2.192	2.337
0.4	-5.508	-4.231	-0.922	1.643	2.317	2.543
0.45	-5.515	-4.493	-1.445	1.380	2.210	2.497
0.5	-5.592	-4.725	-1.896	0.932	1.799	2.104
0.55	-5.752	-4.959	-2.305	0.257	1.017	1.282
0.6	-6.012	-5.221	-2.750	-0.746	-0.219	-0.042
0.65	-6.399	-5.539	-3.389	-2.251	-2.041	-1.979
0.7	-6.950	-5.968	-4.524	-4.569	-4.714	-4.773
0.75	-7.735	-6.663	-6.746	-8.316	-8.844	-9.029

Table 3.5.2 T-stress T/σ^* for the Brazilian disk test ($\sigma^*=P/(\pi tR)$).

$\alpha = a/2R$	$\Theta = \pi/16$	$\pi/8$	$\pi/4$	$3\pi/8$	$7\pi/16$	$\pi/2$
0	-1.228	-1.228	-1.228	-1.228	-1.228	-1.228
0.05	-0.608	-1.062	-1.196	-1.220	-1.224	-1.225
0.1	0.549	-0.594	-1.087	-1.188	-1.204	-1.209
0.15	1.446	0.019	-0.900	-1.127	-1.166	-1.178
0.2	1.995	0.600	-0.651	-1.036	-1.106	-1.128
0.25	2.301	1.053	-0.372	-0.914	-1.021	-1.054
0.3	2.455	1.358	-0.104	-0.769	-0.910	-0.955
0.35	2.510	1.529	0.118	-0.610	-0.776	-0.830
0.4	2.500	1.591	0.276	-0.449	-0.622	-0.679
0.45	2.440	1.570	0.367	-0.297	-0.457	-0.510
0.5	2.342	1.486	0.400	-0.158	-0.289	-0.332
0.55	2.209	1.354	0.394	-0.034	-0.127	-0.156
0.6	2.043	1.190	0.369	0.076	0.021	0.004
0.65	1.843	1.005	0.345	0.173	0.147	0.139
0.7	1.608	0.814	0.334	0.255	0.247	0.245
0.75	1.337	0.636	0.343	0.320	0.320	0.321
1	0.423	0.423	0.423	0.423	0.423	0.423

Table 3.5.3 Biaxiality ratio $\beta(1\text{-}a/D)^{1/2}$ for the Brazilian disk test.

3.6 Round-CT specimen

The RCT-specimen is identical with the single-edge-cracked circular disk, if the load application holes are neglected. Figure 3.6.1 represents this fracture mechanics test specimen.

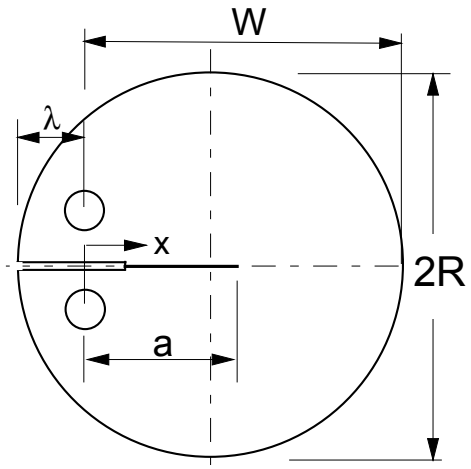

Fig. 3.6.1 Geometric data of the RCT specimen.

The stress intensity factor solution was derived by Newman [26] as

$$K_I = \frac{P}{B\sqrt{W}} Y^*(\alpha) \ , \quad \alpha = a / W \tag{3.6.1a}$$

$$Y^* = \frac{(2+\alpha)(0.76 + 4.8\alpha - 11.58\alpha^2 + 11.43\alpha^3 - 4.08\alpha^4}{(1-\alpha)^{3/2}} \tag{3.6.1b}$$

For $0.2 \le \alpha \le 0.8$ the weight function can be expressed by the polynomial [27]

$$h = \sqrt{\frac{2}{\pi a}} \frac{1}{\sqrt{1 - x/a}\,(1-\alpha)^{3/2}} [(1-\alpha)^{3/2} + \sum D_{nm} (1 - x/a)^{m+1} \alpha^n] \tag{3.6.2}$$

with the coefficients listed in Table 3.6.1

n	m=0	1	2	3	4
0	2.826	-5.865	0.8007	-0.2584	0.6856
1	-10.948	48.095	-3.839	1.280	-6.734
2	35.278	-143.789	6.684	-5.248	25.188
3	-41.438	196.012	-4.836	11.435	-40.140
4	15.191	-92.787	-0.7274	-7.328	22.047

Table 3.6.1 Coefficients D_{nm} for eq.(3.6.2)

The T-stress term can be approximated by

$$T \cong 0.948 \frac{P}{B} \frac{a}{(a+\lambda)^2} \tag{3.6.3}$$

4 Double-edge-cracked circular disk

The double-edge-cracked circular disk is shown in Fig. 4.1. Different traction and displacement boundary conditions are possible. They will be considered in the following sections.

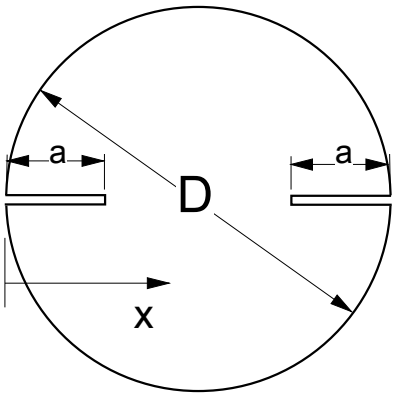

Fig. 4.1 Double-edge-notched disk.

4.1 Traction boundary conditions

Pure traction loading of $\sigma_n = \sigma_R$ =constant and $\tau_{R\omega} = 0$ is illustrated in Fig. 4.1.1.

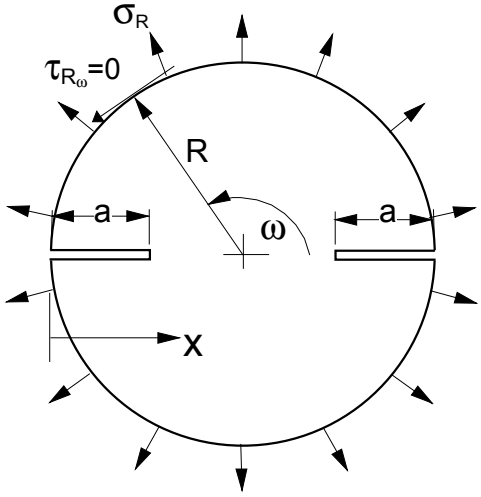

Fig. 4.1.1 Double-edge-cracked disk under traction boundary conditions of $\sigma_n=\sigma_R$=constant, $\tau_{R\omega}=0$.

The geometric function *F* for the stress intensity factor is

$$K = \sigma_n F\sqrt{\pi a} \quad , \quad F' = F\sqrt{1-\alpha}\ , \alpha = a / R \tag{4.1.1}$$

as shown in Fig. 4.1.2 and approximated by

$$F = \frac{1.1215 + 0.2746\,\alpha - 0.7959\,\alpha^2 - 1.1411\,\alpha^3 + 1.1776\,\alpha^4}{\sqrt{1-\alpha}} \tag{4.1.2}$$

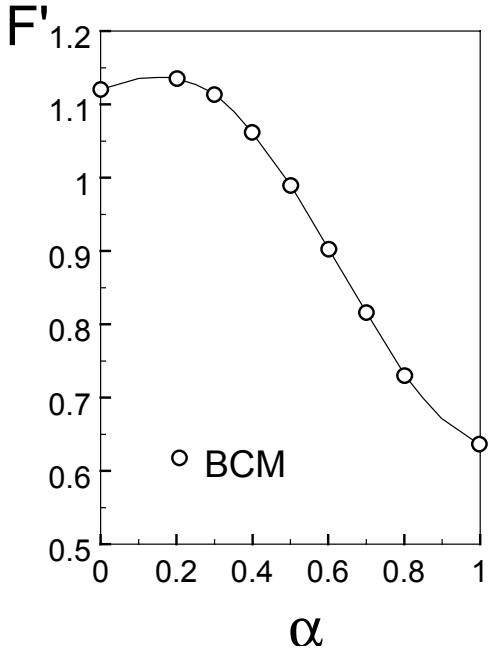

Fig. 4.1.2 Geometric function F' for the double-edge-cracked disk.

The weight function for the double-edge-cracked disk under traction boundary conditions is

$$h = \sqrt{\frac{2}{\pi a}}\left[\frac{1}{\sqrt{1-\rho}} + C_0\sqrt{1-\rho} + C_1(1-\rho)^{3/2} + C_2(1-\rho)^{5/2}\right] \tag{4.1.3}$$

with $\rho = x/a$ and the coefficients

$$C_0 = \frac{0.4594 + 2.3454\,\alpha - 1.0205\,\alpha^2 - 7.7547\,\alpha^3 + 9.1403\,\alpha^4}{\sqrt{1-\alpha}} \tag{4.1.4}$$

$$C_1 = \frac{0.6833 - 0.1484\,\alpha - 1.8811\,\alpha^2 + 7.0112\,\alpha^3 - 8.9802\,\alpha^4}{\sqrt{1-\alpha}} \tag{4.1.5}$$

$$C_2 = \frac{-0.3059 + 0.2829\,\alpha + 0.3552\,\alpha^2 - 1.9646\,\alpha^3 + 2.4682\,\alpha^4}{\sqrt{1-\alpha}} \tag{4.1.6}$$

The T-stress under loading by constant circumferential normal tractions σ_n is shown in Fig. 4.1.3 together with the biaxiality ratio β. In contrast to the single-edge-cracked disk, the relative crack length is defined here by $\alpha = a/R$ ($R = D/2$).

The T-stress can be expressed by

$$\frac{T}{\sigma_n} = 0.474 + 0.4022\,\alpha + 0.9104\,\alpha^2 + 1.4406\,\alpha^3 - 1.6874\,\alpha^4 \qquad (4.1.7)$$

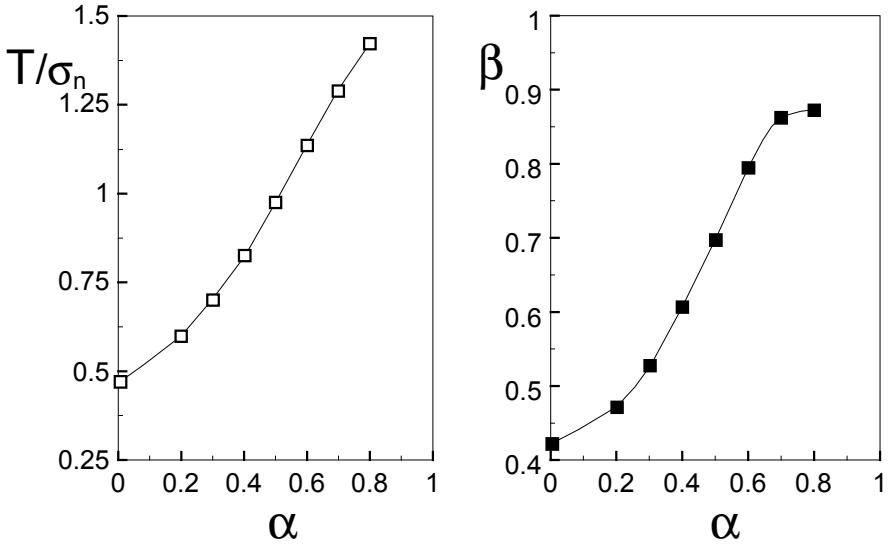

Fig. 4.1.3 T-stress and biaxiality ratio for the double-edge-cracked circular disk under circumferential normal tractions.

For the Green's function under symmetrical loading the same set-up is chosen as used for single-edge-cracked components. It can be expressed in the integrated form as

$$T = C\int_0^a (1 - x/a)\,\sigma_y(x)\,dx - \sigma_y\big|_{x=a} \qquad (4.1.8)$$

with the parameter C entered into Table 4.1.1 and fitted for $\alpha \le 0.8$ by the polynomial

$$C = \frac{1}{a}(0.9481 + 0.8043\,\alpha + 1.8207\,\alpha^2 + 2.8813\,\alpha^3 - 3.3747\,\alpha^4) \qquad (4.1.9)$$

a/R	T/σ_n	β	a·C
0	0.474	0.423	0.9481
0.2	0.599	0.472	1.199
0.3	0.702	0.528	1.405
0.4	0.829	0.604	1.658
0.5	0.977	0.698	1.954
0.6	1.136	0.795	2.273
0.7	1.290	0.865	2.580
0.8	1.425	0.873	2.850

Table 4.1.1 T-stress, biaxiality ratio, and coefficient for the Green's function.
Loading: constant circumferential normal tractions, disappearing shear tractions.

The higher order coefficients A_1 and A^*_1 according to eq.(1.2) are compiled in Table 4.1.2.

a/R	A_1	A^*_1
0.2	-0.039	0.472
0.3	-0.012	0.285
0.4	0.008	0.170
0.5	0.021	0.085
0.6	0.023	0.022
0.7	0.007	-0.016
0.8	-0.051	-0.025

Table 4.1.2 Coefficients A_1 and A^*_1 according to eq.(1.2).

The double-edge-cracked disk under constant shear tractions τ_0 on the crack faces is illustrated in Fig. 4.1.4 together with the stress intensity factor solution represented by

$$K_{II} = \tau_0 F_{II} \sqrt{\pi a}\ , \quad F'_{II} = F_{II} \sqrt{1 - a / R} \tag{4.1.10}$$

The data of Fig. 4.1.4 can be expressed by

$$F_{II} = \frac{1.1215 - 0.5608\,\alpha + 0.2185\,\alpha^2 - 0.5007\,\alpha^3 + 0.3584\,\alpha^4}{\sqrt{1-\alpha}}, \quad \alpha = a / R \tag{4.1.11}$$

In addition, Fig. 4.1.4 contains the mode-II stress intensity factor solution for the double-edge-cracked endless strip [1] as the dashed curve. Only small deviations from this solution are visible in the region of $0.3 < a/R < 0.7$. An approximate weight function can be derived from eq.(4.1.11) by applying the extended Petroski-Achenbach procedure ([28], see also [6]).

The coefficients for a representation

$$h_{II} = \sqrt{\frac{2}{\pi a}}\left[\frac{1}{\sqrt{1-\rho}} + C_1\sqrt{1-\rho} + C_1(1-\rho)^{3/2} + C_2(1-\rho)^{5/2}\right] \tag{4.1.12}$$

are compiled in Table 4.1.3

α	C_0	C_1	C_2
0.2	0.496	0.693	-0.306
0.3	0.553	0.680	-0.299
0.4	0.646	0.647	-0.286
0.5	0.807	0.560	-0.258
0.6	1.103	0.344	-0.195
0.7	1.700	-0.190	-0.049

Table 4.1.3 Coefficients for the weight function eq.(4.1.12).

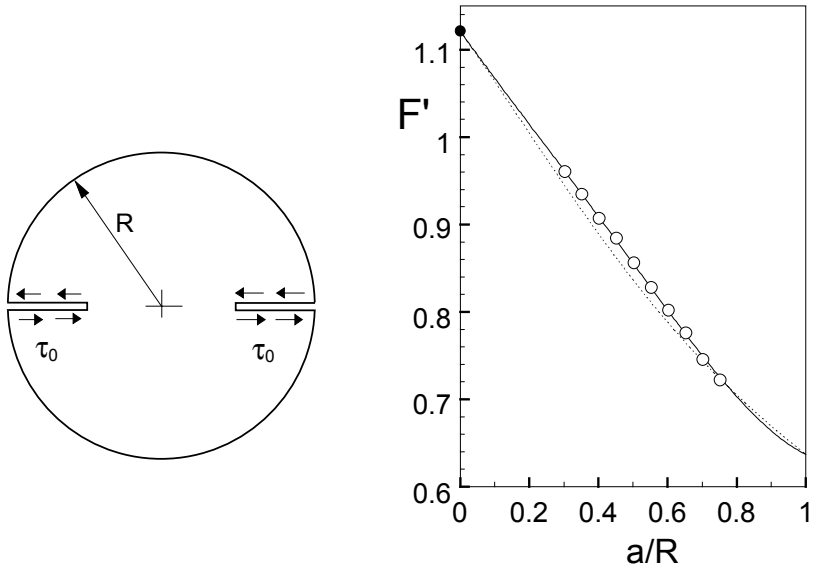

Fig. 4.1.4 Double-edge-cracked disk under constant shear tractions on the crack faces; dashed curve: solution for the double-edge-cracked endless strip (see e.g. [1]).

Figure 4.1.5 represents the displacements under constant normal tractions σ_n in the form

$$\delta = \frac{2a\sigma_n}{E'}\frac{1}{\alpha}\ln\frac{1}{1-\alpha}\lambda(\alpha) \ , \quad \alpha = a/R \tag{4.1.13}$$

The results of boundary collocation computations are represented by the circles. From a least-squares fit we obtain the representation

$$\lambda = 1.454 + 0.3893\,\alpha + 5.0022\,\alpha^2 - 19.5054\,\alpha^3 + 23.6198\,\alpha^4 - 10.3233\,\alpha^5 \tag{4.1.14}$$

The dashed curve in Fig. 4.1.5 is the solution for the double-edge-cracked endless parallel strip as reported by Tada [1].

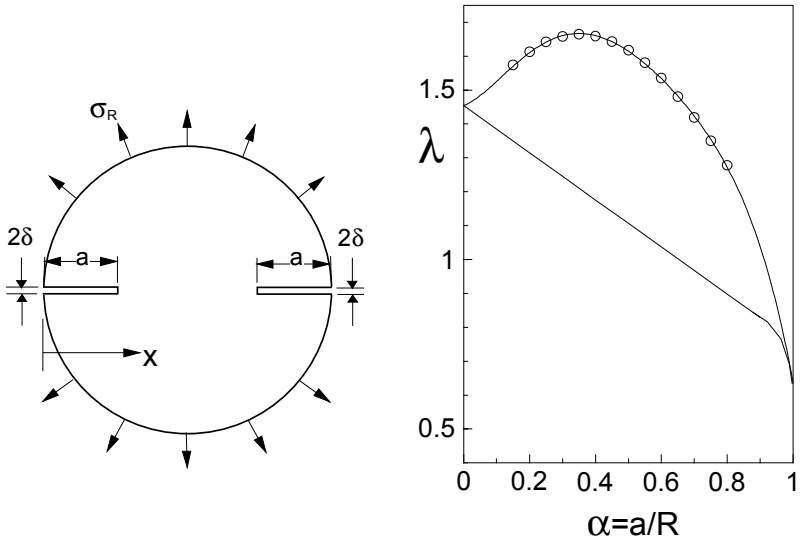

Fig. 4.1.5 Crack-mouth displacements ($x = 0$) according to eq.(4.1.13); circles: double-edge-cracked disk, dashed curve: results for the double-edge-cracked endless parallel strip, reported by Tada [1].

4.2 Mixed boundary conditions

Figure 4.2.1 shows the case of constant normal tractions σ_R and disappearing tangential displacements v_R along the circumference.

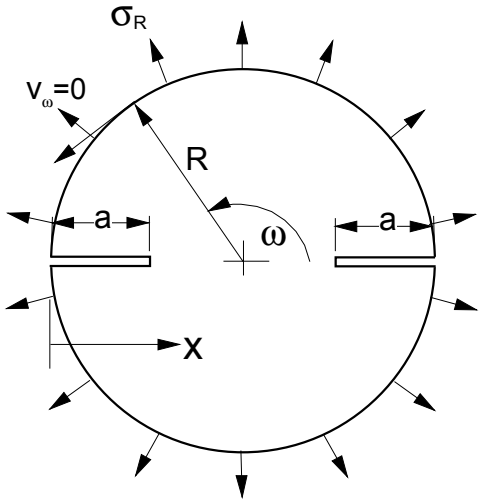

Fig. 4.2.1 Mixed boundary conditions σ_n=constant, v_ω=0.

The stress intensity factor described by

$$K = \sigma_n F(\nu, a / R)\sqrt{\pi a} \tag{4.2.1}$$

and the T-stress are plotted in Fig. 4.2.2. In this loading case the T-stresses are very small. The higher order terms A_1 and A^*_1 of eq.(1.2) are compiled in Tables 4.2.1 and 4.2.2.

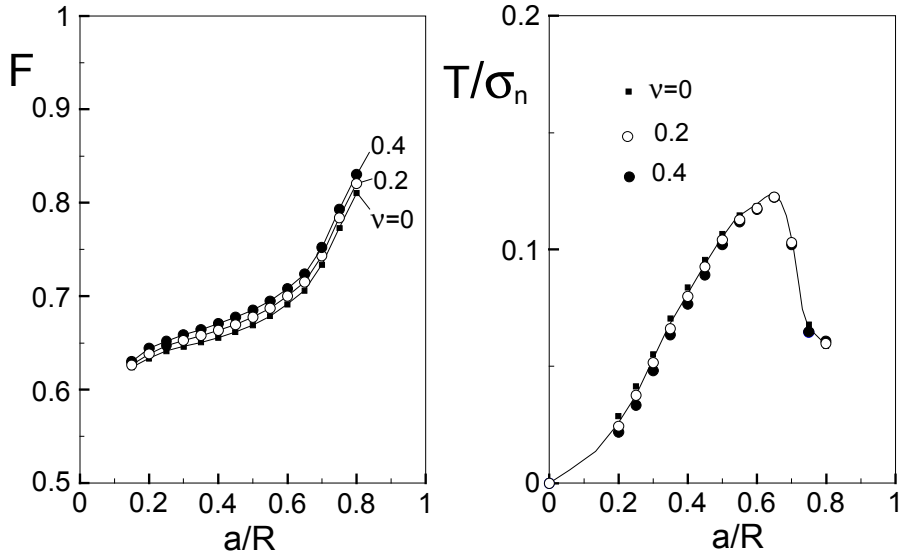

Fig. 4.2.2 Geometric function F and T-stress as functions of ν and a/R.

For $\nu = 0.25$ and $\alpha = a/R \le 0.75$ the geometric function can be approximated by

$$F = 0.59 + 0.462\alpha - 1.171\alpha^2 + 1.197\alpha^3 \tag{4.2.2}$$

and the related T-stress for $\alpha \le 0.75$ by

$$T / \sigma^* = 0.127\alpha^2 + 5.024\alpha^3 - 18.468\alpha^4 + 26.0173\alpha^5 - 13.7978\alpha^6 \qquad (4.2.3)$$

a/R	ν=0	0.2	0.4
0.2	-0.172	-0.172	-0.171
0.3	-0.137	-0.137	-0.137
0.4	-0.119	-0.118	-0.118
0.5	-0.108	-0.107	-0.107
0.6	-0.104	-0.103	-0.102
0.7	-0.108	-0.107	-0.107
0.8	-0.127	-1.27	-0.126

Table 4.2.1 Coefficient A_1 according to eq.(1.2).

a/R	ν=0	0.2	0.25	0.4
0.2	0.011	0.009	-0.008	-0.014
0.3	-0.035	-0.041	-0.043	-0.048
0.4	-0.038	-0.045	-0.046	-0.051
0.5	-0.039	-0.047	-0.049	-0.053
0.6	-0.038	-0.045	-0.047	-0.051
0.7	-0.029	-0.034	-0.035	-0.039
0.8	-0.017	-0.022	-0.023	-0.026

Table 4.2.2 Coefficient A^*_1 according to eq.(1.2).

Figure 4.2.3 shows the case of constant radial displacements $u_n = u_R$ and disappearing shear tractions $\tau_{R\omega}$. The stress intensity factor is given by

$$K = \sigma^* F(\nu, a/R)\sqrt{\pi a}\,, \quad \sigma^* = \frac{u_R E}{R} \qquad (4.2.4)$$

The geometric function F is plotted in Fig. 4.2.4a. In the form of

$$F^* = F(1-\nu) \qquad (4.2.5)$$

the results (which now coincide for $a/R = 0$) are shown in Fig. 4.2.4b.
For $\nu = 0.25$ the geometric function F in the region $a/R \le 0.8$ can be approximated by

$$F = \tfrac{4}{3} + 0.8251\alpha + 0.65527\alpha^2 - 12.6637\alpha^3 + 17.6804\alpha^4 - 7.1736\alpha^5 \qquad (4.2.6)$$

and the T-term by

$$T / \sigma^* = -0.9611\alpha^2 + 11.812\alpha^3 - 23.8847\alpha^4 + 20.5897\alpha^5 - 6.7657\alpha^6 \qquad (4.2.7)$$

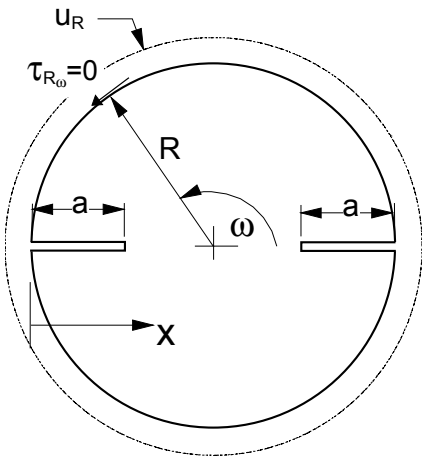

Fig. 4.2.3 Mixed boundary conditions u_R =constant, $\tau_{R\omega}=0$.

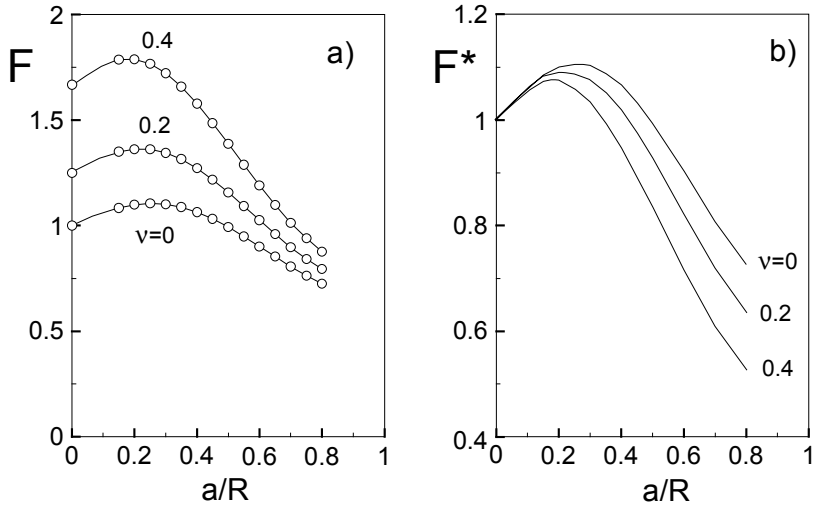

Fig. 4.2.4 Geometric function according to eq.(4.2.4).

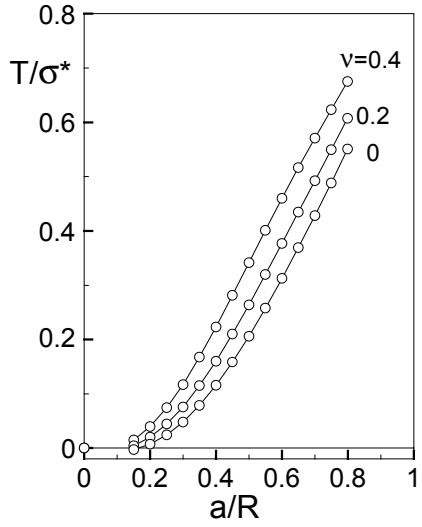

Fig. 4.2.5 T-stress term for the conditions of u_R =constant, $\tau_{R\omega}=0$.

Values of the higher order coefficients A_1 and A^*_1 of eq.(1.2) are compiled in Tables 4.2.3 and 4.2.4.

a/R	ν=0	0.2	0.25	0.4
0.2	-0.094	-0.116	-0.122	-0.149
0.3	-0.064	-0.075	-0.079	-0.094
0.4	-0.041	-0.047	-0.049	-0.055
0.5	-0.025	-0.027	-0.028	-0.030
0.6	-0.016	-0.016	-0.016	-0.017
0.7	-0.015	-0.015	-0.015	-0.016
0.8	-0.027	-0.030	-0.030	-0.033

Table 4.2.3 Coefficient A_1 according to eq.(1.2).

a/*R*	ν=0	0.2	0.4
0.2	0.003	0.002	0.001
0.3	0.007	0.006	0.004
0.4	0.010	0.008	0.007
0.5	0.011	0.009	0.008
0.6	0.010	0.008	0.007
0.7	0.007	0.006	0.004
0.8	0.003	0.003	0.002

Table 4.2.4 Coefficient A^*_1 according to eq.(1.2).

Figure 4.2.6 represents the crack opening displacements δ (for δ see Fig. 4.1.5) under constant radial displacements and disappearing shear tractions at the circumference in the form

$$\delta = \frac{2a\sigma^*}{E'}\lambda(a/R) \tag{4.2.8}$$

with σ* given by eq.(4.2.4).

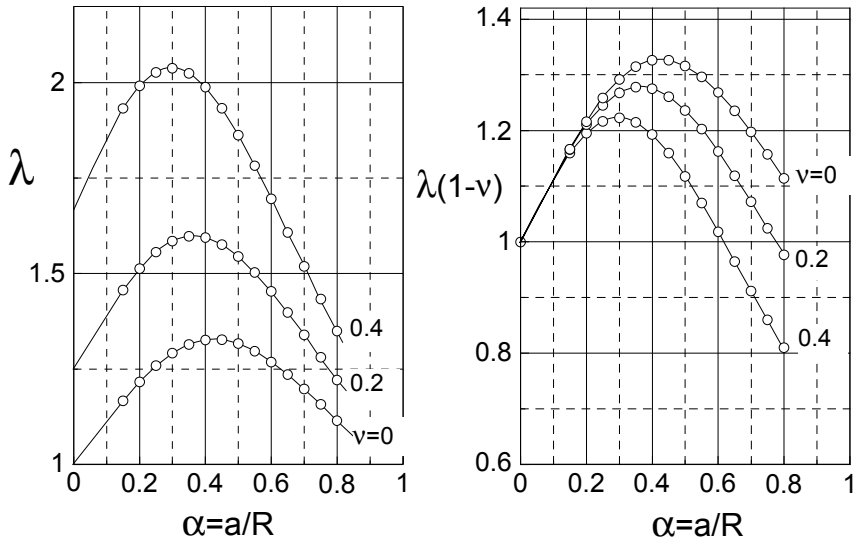

Fig. 4.2.6 Crack-mouth displacement represented by eq.(4.2.8). Boundary conditions: u_R = constant, $\tau_{R\omega} = 0$.

4.3 Displacement boundary conditions

The case of pure displacement boundary conditions is illustrated in Fig. 4.3.1. Under these boundary conditions, the geometric functions F for the stress intensity factor, defined by eq.(4.2.3), result as shown in Fig. 4.3.2a. The T-stress term is given in Fig. 4.3.2b.

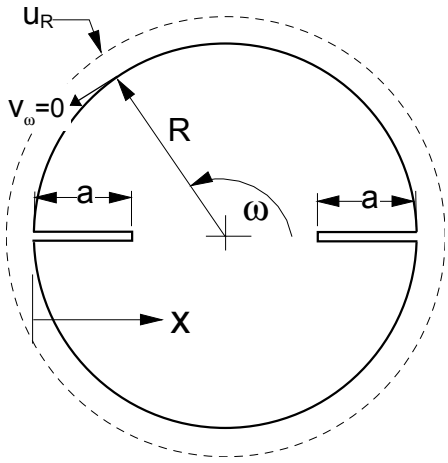

Fig. 4.3.1 Displacement boundary conditions u_R =constant, v_ω=0.

For $\nu = 0.25$ the geometric function F in the range $a/R \le 0.8$ can be approximated by

$$F = 0.824 - 0.1267\,\alpha + 0.02799\,\alpha^2 \tag{4.3.1}$$

and the T-stress in the range of $0.2 \le a/R \le 0.8$ by

$$T / \sigma^* = 0.0496 + 0.175\,\alpha - 0.1016\,\alpha^2 - 0.2251\,\alpha^3 + 0.5331\,\alpha^4 \tag{4.3.2}$$

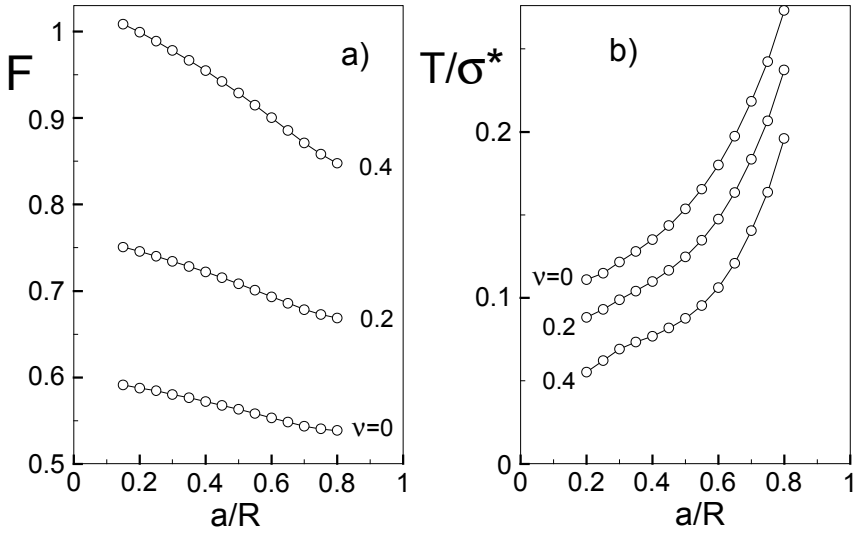

Fig. 4.3.2 Geometric function *F* and T-stress as functions of ν and *a*/*R*.

a/R	ν=0	0.2	0.25	0.4
0.2	-0.170	-0.212	-0.226	-0.282
0.3	-0.138	-0.172	-0.183	-0.228
0.4	-0.119	-0.148	-0.158	-0.195
0.5	-0.106	-0.132	-0.140	-0.172
0.6	-0.096	-0.119	-0.126	-0.154
0.7	-0.090	-0.111	-0.117	-0.142
0.8	-0.090	-0.110	-0.117	-0.140

Table 4.3.1 Coefficient A_1 according to eq.(1.2).

a/R	ν=0	0.2	0.25	0.4
0.2	0.239	0.237	0.232	0.23
0.3	0.167	0.171	0.174	0.188
0.4	0.130	0.138	0.141	0.156
0.5	0.106	0.114	0.117	0.133
0.6	0.085	0.093	0.096	0.110
0.7	0.065	0.072	0.074	0.085
0.8	0.043	0.048	0.050	0.056

Table 4.3.2 Coefficient A^*_1 according to eq.(1.2).

4.4 Double-edge-cracked Brazilian disk

The Brazilian disk test with a double-edge-cracked circular disk is illustrated by Fig. 4.4.1.

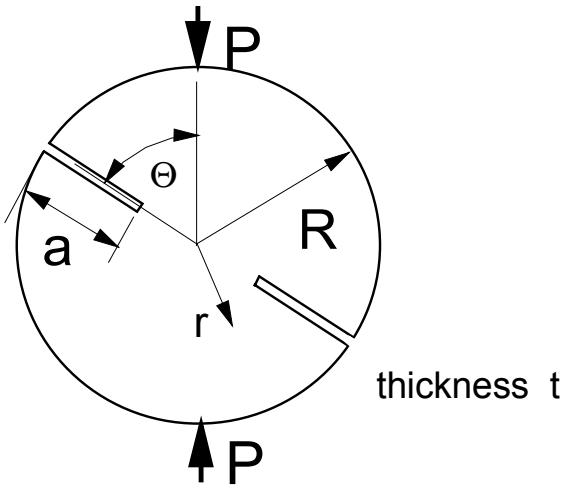

Fig. 4.4.1 Brazilian disk test with double-edge-cracked specimen.

Mode-I stress intensity factors computed with the weight function, eqs.(4.1.3)-(4.1.6), and expressed by the geometric function F are entered into Table 4.4.1. The geometric function F is defined by

$$K = \sigma^* F\sqrt{\pi a} \quad , \quad \sigma^* = P/(\pi R t) \tag{4.4.1}$$

$\alpha = a/R$	$\Theta = \pi/32$	$\pi/16$	$\pi/8$	$\pi/4$	$3\pi/8$	$7\pi/16$	$\pi/2$
0	0	0	0	0	0	0	0
0.1	-6.189	-2.953	-0.970	-0.304	-0.180	-0.160	-0.154
0.2	-4.105	-3.312	-1.709	-0.648	-0.399	-0.357	-0.344
0.3	-2.728	-2.680	-1.989	-0.987	-0.652	-0.590	-0.571
0.4	-1.901	-2.044	-1.927	-1.274	-0.927	-0.854	-0.832
0.5	-1.343	-1.541	-1.713	-1.479	-1.212	-1.145	-1.127
0.6	-0.934	-1.153	-1.469	-1.607	-1.500	-1.459	-1.445
0.7	-0.615	-0.855	-1.263	-1.705	-1.809	-1.817	-1.817

Table 4.4.1 Stress intensity factor represented by the geometric function F for the Brazilian disk test.

Using the Green's function and the stress distribution given by eqs.(3.5.1) and (3.5.2), the T-stress was computed. Table 4.4.2 contains the data for several angles Θ (see Fig. 4.4.1).

$\alpha = a/R$	$\Theta = \pi/32$	$\pi/16$	$\pi/8$	$\pi/4$	$3\pi/8$	$7\pi/16$	$\pi/2$
0	0	0	0	0	0	0	0
0.1	-3.075	1.859	1.076	0.376	0.227	0.203	0.195
0.2	-8.879	-2.012	1.084	0.756	0.509	0.462	0.447
0.3	-8.773	-4.696	-0.096	0.995	0.825	0.773	0.756
0.4	-8.009	-5.678	-1.584	0.969	1.139	1.123	1.114
0.5	-7.348	-5.934	-2.788	0.649	1.403	1.484	1.504
0.6	-6.833	-5.924	-3.601	0.118	1.571	1.818	1.891
0.7	-6.42	-5.81	-4.10	-0.484	1.62	2.08	2.23
0.8	-6.07	-5.65	-4.36	-1.02	1.56	2.23	2.46

Table 4.4.2 T-stress T/σ^* for the Brazilian disk test ($\sigma^*=P/(\pi Rt)$).

References

[1] Tada, H., Paris, P.C., Irwin, G.R., The stress analysis of cracks handbook, Del Research Corporation, 1986.

[2] Sih, G.C., Handbook of stress intensity factors, Institute of Fracture and Solid Mechanics, Lehigh University, Bethlehem, Pennsylvania, 1973.

[3] Rooke, D.P., Cartwright, Her Majesty's Stationery Office, London, 1974.

[4] Murakami, Y., et al., Stress intensity factors handbook, Pergamon Press, 1986.

[5] Wu, X.R., Carlsson, A.J., Weight functions and stress intensity factor solutions, Pergamon Press, Oxford 1991.

[6] Fett, T., Munz, D., Stress intensity factors and weight functions, Computational Mechanics Publications, Southampton, 1997.

[7] Williams, M.L., On the stress distribution at the base of a stationary crack, J. Appl. Mech. **24**(1957), 109-114.

[8] Leevers, P.S., Radon, J.C., Inherent stress biaxiality in various fracture specimen geometries, Int. J. Fract. **19**(1982), 311-325.

[9] Kfouri, A.P., Some evaluations of the elastic T-term using Eshelby's method, Int. J. Fract. **30**(1986), 301-315.

[10] Sham, T.L., The theory of higher order weight functions for linear elastic plane problems, Int. J. Solids and Struct. **25**(1989), 357-380.

[11] Sham, T.L., The determination of the elastic T-term using higher order weight functions, Int. J. Fract. **48**(1991), 81-102.

[12] Fett, T., A Green's function for T-stresses in an edge-cracked rectangular plate, Eng. Fract. Mech. **57**(1997), 365-373.

[13] Fett, T., T-stresses in rectangular plates and circular disks, Engng. Fract. Mech. **60**(1998), 631-652.

[14] Wang, Y.Y., Parks, D.M., Evaluation of the elastic T-stress in surface-cracked plates using the line-spring method, Int. J. Fract **56**(1992), 25-40.

[15] Sherry, A.H., France, C.C., Goldthorpe, M.R., Compendium of T-stress solutions for two and three- dimensional cracked geometries, Engng. Fract. Mech. **18**(1995), 141-155.

[16] Bückner, H., A novel principle for the computation of stress intensity factors, ZAMM **50** (1970), 529-546.

[17] Rice, J.R., Some remarks on elastic crack-tip stress fields, Int. J. Solids and Structures **8**(1972), 751-758.

[18] Fett, T., T-stresses for components with one-dimensional cracks, Report FZKA 6170, Forschungszentrum Karlsruhe, 1998.

[19] Atkinson, C., Smelser, R.E., Sanchez, J., Combined mode fracture via the cracked Brazilian disk test, Int. J. Fract. **18**(1982), 279-291

[20] Awaji, H., Sato, S., Combined mode fracture toughness measurement by the disk test, J. Engng. Mat. Tech. **100**(1978), 175-182.

[21] Fett, T., Mode-II weight function for circular disks with internal radial crack and application to the Brazilian disk test, Int. J. Fract. **89**(1998), L9-L13.

[22] Fett, T., Stress intensity factors and weight functions for special crack problems, Report FZKA 6025, Forschungszentrum Karlsruhe, 1998.

[23] Fett, T., T-stresses for components with one-dimensional cracks, FZKA 6170, Forschungs-zentrum Karlsruhe, 1998.

[24] Sato, S., Kawamata, K., Combined-mode fracture toughness of reactor-grade graphite at high temperature, High Temp.-High Press. **12**(1980), 23-32.

[25] Wigglesworth, L.A., Stress distribution in a notched plate, Mathematica **4**(1957), 76-96.

[26] Newman, J.C., Stress intensity factors and crack opening displacements for round compact specimens, Int. J. Fract. **17**(1981) 567-578.

[27] Fett, T., A weight function for the RCT-specimen, Int. J. Fract. **63**(1993) R81-R85.

[28] Petroski, H.J., Achenbach, J.D., Computation of the weight function from a stress intensity factor, Engng. Fract. Mech. **10**(1978), 257.